MONOLITHIC CATALYST BEDS FOR HYDRAZINE REACTORS

Interim Report

November 12, 1969, Through April 12, 1971

71-R-259

Contract NAS 7-755

Prepared By:

Rocket Research Corporation
Redmond, Washington 98052

For:

National Aeronautics and Space Administration
Ames Research Center, Moffett Field, California

and

Jet Propulsion Laboratory
Pasadena, California

MONOLITHIC CATALYST BEDS FOR HYDRAZINE REACTORS

Interim Report

November 12, 1969, Through April 12, 1971

71-R-259

Contract NAS 7-755

Prepared By:

Rocket Research Corporation
Redmond, Washington 98052

For:

National Aeronautics and Space Administration
Ames Research Center, Moffett Field, California

and

Jet Propulsion Laboratory
Pasadena, California

TABLE OF CONTENTS

TABLE OF CONTENTS (Concluded)

LIST OF FIGURES

LIST OF TABLES

1.0 INTRODUCTION AND SUMMARY

Rocket Research Corporation (RRC) under NASA Contract NAS 7-755 has carried out research aimed at the development of a monolithic catalyst bed for monopropellant hydrazine decomposition. This interim technical report covers work performed during the period from November 12, 1969, to April 12, 1971. The program involved the exploring of a new hydrazine catalyst concept wherein open-celled foamed materials are used as supports for the active catalysts. Upon the open-celled foamed material is deposited a high-surface-area material. This material is then coated with an active metal to provide a spontaneous catalyst.

The monolithic catalyst offers a single-piece catalyst bed as opposed to current catalysts which are packed into the reactor in granular form. It is hoped that the monolithic nature of the catalyst will result in reduced catalyst attrition as compared to present granular catalyst beds. Additionally, the monolithic catalyst offers the potential of increased bed conductivity, lower bed pressure drop, and simplified reactor assembly procedures.

After initial laboratory screening tests measuring foam metal compatibility with the exhaust gases, crush strength, pressure drop, active surface area, hydrogen chemisorption values, and ignition delay of candidate catalyst configurations, reactor tests were conducted under altitude conditions in a 2.2-N (0.5-lbf) thruster. Foam metal pore size, foam metal density, ceramic coating loading, and active metal loading were varied to optimize engine response and stability of operation. Results of this test program and problems encountered in ceramic material adherence to the foam metal as well as foam metal nitriding problems are discussed herein.

At the end of the reporting period discussed herein, a monolithic catalyst had been successfully tested in the 2.2-N (0.5-lbf) engine for an accumulated burn time of 7,700 seconds and 16 ambient temperature starts. Catalyst condition at the end of this time was entirely satisfactory, with no sign of significant degradation. While not yet attaining the overall activity of Shell 405, the research described herein gives promise that subsequent work will yield a catalyst of long-life potential.

(Reverse side blank)

2.0 MONOLITHIC CATALYST PROPERTIES

The monolithic catalyst bed concept explored by RRC under the contract described herein involves a large number of variables which must be explored to obtain a satisfactory catalyst. The major mechanical and chemical characteristics that are expected to influence the overall performance of such catalysts include:

a. Foam void volume including pore size, pore size distribution, foam ligament thickness, porous surface area, and ligament porosity

b. Foam material properties including thermal conductivity, heat capacity, melting point, coefficient of thermal expansion, chemical inertness, and crush strength

c. Surface coating characteristics including surface area, adherence to metal matrix, and surface area degradation at high temperatures

d. Active metal coating including the chemical nature of the active metal, quantity of active metal deposited, method of active metal deposition, and hydrogen chemisorption value of the final catalyst.

The foam catalyst bed properties are discussed in detail in the ensuing sections.

2.1 FOAM MATERIALS

2.1.1 Structure of the Foam Matrix

The substratum for deposition of an active surface area coating and active metal is an open-celled, hollow ligament metal foam. Photomicrography of typical foam structures prior to application of any coating are shown in Figures 2-1 and 2-2. The repeating unit in this structure, the cell unit, is that of a dodecahedron with pentagonal windows. The strands, or ligaments, connecting the nodes typically have a triangular cross section and are hollow. This foam structure is designated the 200 series by the manufacturer, Astro-Met Associates, Incorporated.* The picture in Figure 2-1 was focused on the upper part of the sample to show the hollow ligaments protruding where the foam was cut to shape.

Another metal foam type with a more irregular structure called 300 series is also available, but initial tests showed that these porous metals have an excessively high pressure drop. The nomenclature of foam types, pore size, and density used in this report is described in the appendix to this volume.

The foam structure is generally described by two numbers: the average pore diameter and the percent void contained in a unit volume. More frequently, the percent density is used which is equal

*Astro-Met Associates, Incorporated, 95 Barron Drive, Cincinnati, Ohio.
John W. Graham, President

PHOTOMICROGRAPH OF 20 MIL PORE SIZE TUNGSTEN FOAM

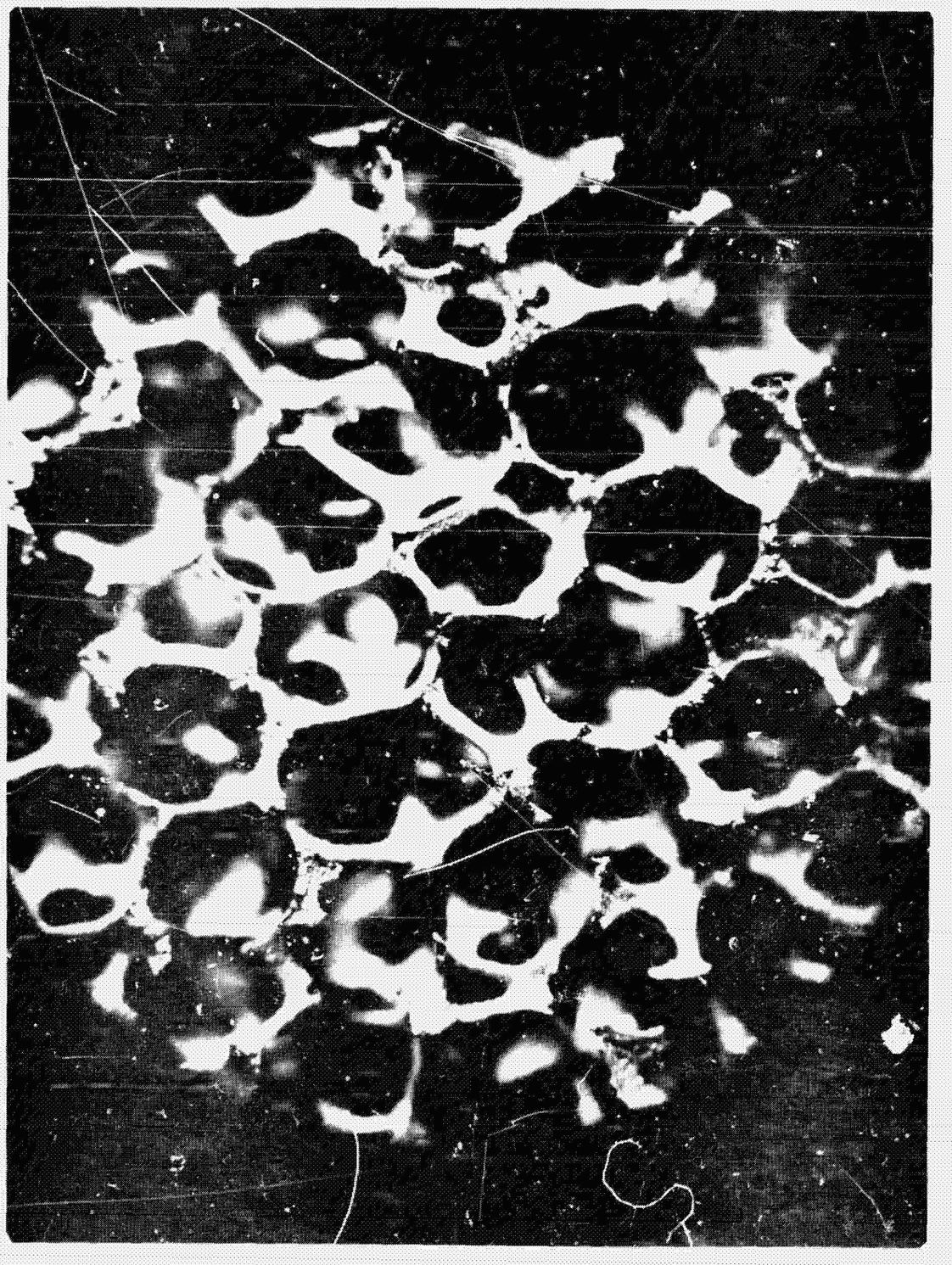

Magnification 37X

56000-33

Figure 2-1

COMPARISON OF 10 MIL (LEFT)
AND 20 MIL (RIGHT) PORE SIZE TUNGSTEN FOAM

Magnification 37X

56000-33

Figure 2-2

to 100% minus percent void volume. Typical pore diameters used in the monolithic catalyst program were 500 μm (0.020 inch) to 250 μm (0.010 inch). Densities ranged from 3 to 10%. Metal foams are also frequently characterized by giving the number of pores per inch instead of the pore diameter.

Since the initiation of the program described herein, other foam metals have become available on the market with solid ligaments and/or different cell shapes. However, little characterization or testing has been accomplished with these metals; and the foam metal used in this program was limited to that supplied by Astro-Met Associates, Incorporated.

An important requirement for monolithic catalysts is the uniformity of the foam structure. Closed pores or variations in density or pore size can cause the flow to channel along the path of lower resistance. Uniformity of foam samples was inspected by two methods, including (1) sectioning and visual examination or weighing and (2) taking X-ray photographs. In a few instances irregularities of the foam structure such as closed pores were noted when block specimens were machined to size. These solid metal nodules are also clearly visible in Figure 2-3, which shows an X-ray picture of a block of Hastelloy X from which six cylinders were already cut. Figure 2-4 for comparison shows X-ray photographs of a 250-μm (10-mil) pore size Hastelloy X foam in which the samples were completely uniform in composition.

X-ray pictures were also taken from catalyst samples with aluminum oxide and active metal deposited. However, only very little X-ray absorption is caused by the catalytic coating, and it was not possible to judge the openness of the final prepared catalyst by X-ray techniques.

The sectioning and visual examination technique was mostly applied to post-firing samples, such as the one shown in Figure 2-5 to study uniformity of the coating and quality of adherence. As noted, some pores in this early catalyst sample were inadvertently plugged with coating material.

2.1.2 Melting Point Requirements

The foam material has to withstand reactor temperatures of 1,366°K (2,000°F) for hydrazine propellant without loss of strength. The melting point must also be sufficiently high to avoid melting of the metal. Table 2-1 shows melting points of candidate metals. Some ceramic materials were also considered in this table. However, ceramic foams examined were very fragile and did not offer the advantages found with metal foams. As noted in the table, a large number of the materials are ruled out because they are not compatible with the decomposition products of hydrazine. This incompatibility is manifested in hydrogen embrittlement and/or nitridation resulting in reduced material properties.

2.1.3 Material Compatibility

The most important requirement for candidate foam materials is that of compatibility with the hydrazine exhaust gases under reactor conditions. Titanium, zirconium, columbium, and tantalum (typical high-strength, high-temperature materials) are subject to rapid hydrogen embrittlement in hydrazine exhaust. Nickel, cobalt, iron, and their alloys tend to nitride after extended exposure to

X-RAY PHOTOGRAPH OF HASTELLOY-X 220-7 FOAM WITH METAL NODULES, SAMPLE THICKNESS 0.785 IN.

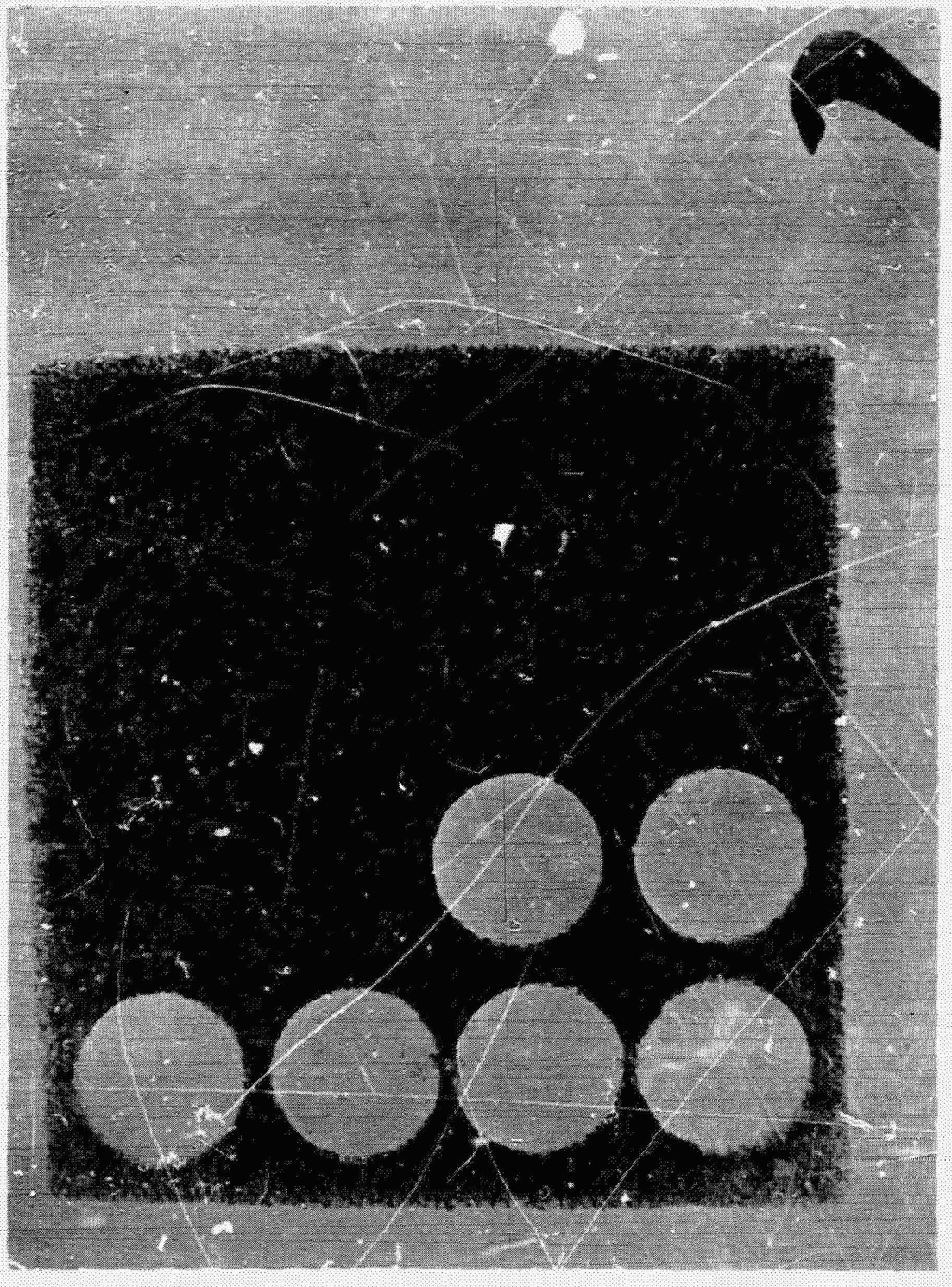

56000-34

Figure 2-3

X-RAY PHOTO OF TWO IDENTICAL HASTELLOY-X 210-7 FOAM SAMPLES.
SAMPLE THICKNESS 0.375 INCH

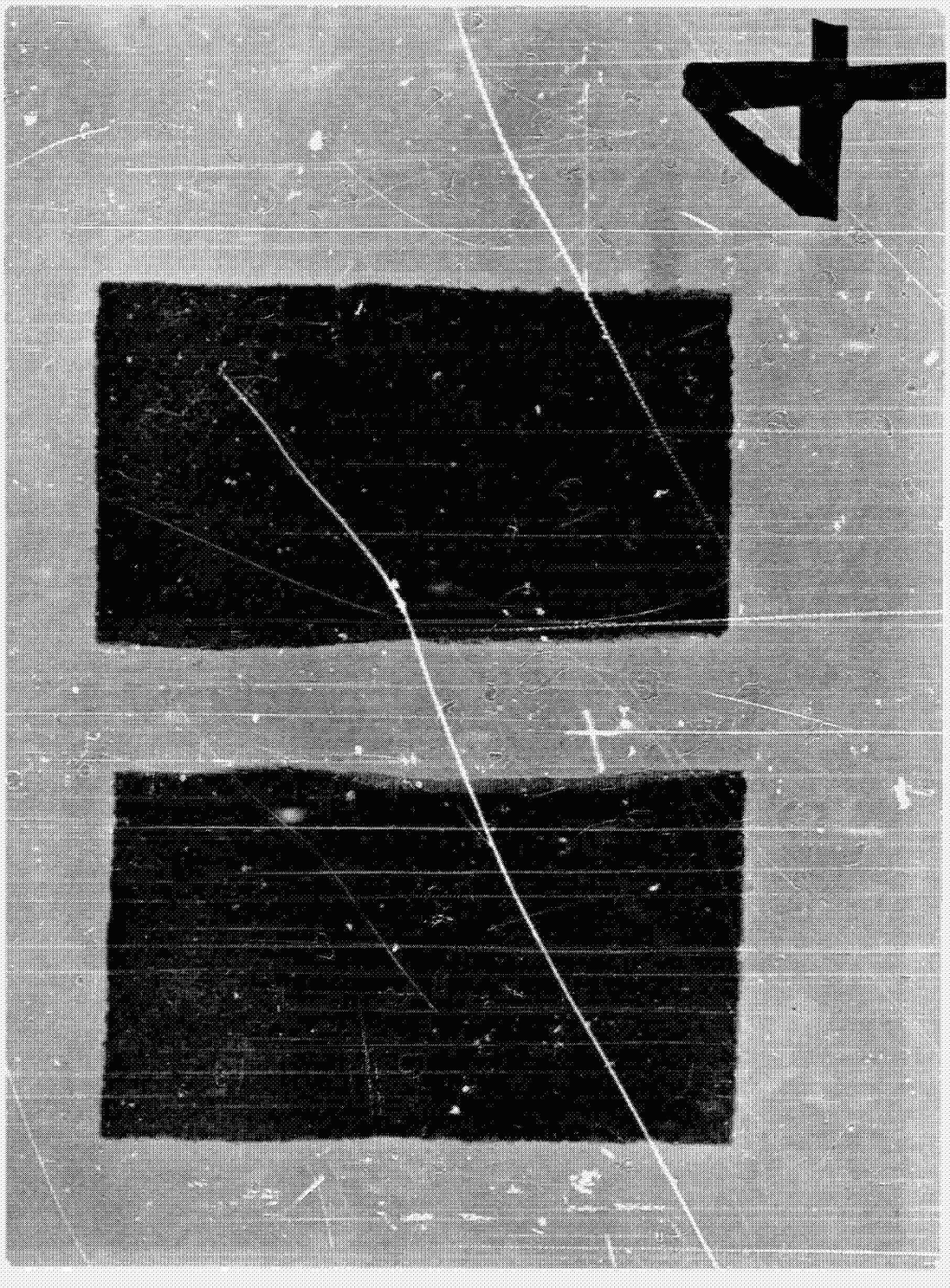

56000-35

Figure 2-4

SECTIONED POST-FIRING MONOLITHIC CATALYST SAMPLE

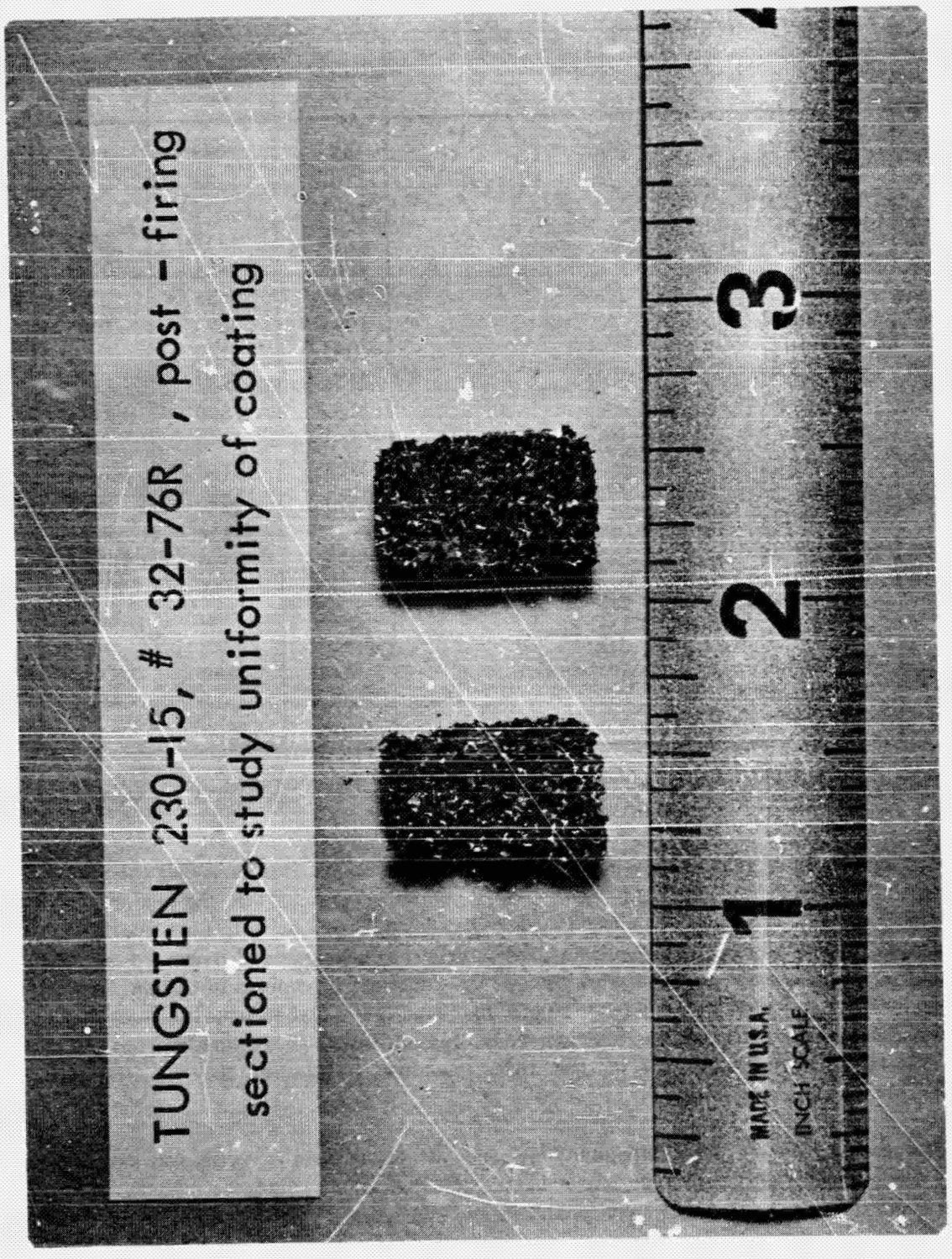

56000-36

Figure 2-5

Table 2-1
MELTING POINT OF CANDIDATE CATALYST BED MATERIALS

	Melting Point		
	°K	°C	°F
Copper	1356	1083	1981
Hastelloy X **	1561	1288	2350
Haynes 25**	1644	1371	2500
Nickel **	1726	1453	2647
Cobalt **	1768	1495	2723
Iron **	1808	1535	2795
Titanium *	1948	1675	3047
Platinum	2042	1769	3216
Zirconium *	2125	1852	3366
Chromium **	2163	1890	3434
Vanadium **	2163	1890	3434
Hafnium *	2423	2150	3900
Iridium	2683	2410	4370
Columbium* (Niobium)	2741	2468	4470
Molybdenum	2883	2610	4730
Zirconium oxide	2988	2715	4920
Aluminum oxide	3253	2980	5400
Tantalum *	3269	2996	5420
Rhenium	3453	3180	5760
Tungsten (Wolfram)	3683	3410	6080
Graphite Sublimes at	3870	3600	6470

*Not compatible with hydrazine exhaust due to hydrogen embrittlement
**Susceptible to nitridation after prolonged exposure

hydrazine exhaust and can only be used for short test durations. This leaves only the noble metals and molybdenum, rhenium, and tungsten as monolithic supports. Where the high cost of noble metals prohibits their large scale use, the choice is thus narrowed down to tungsten, rhenium, and molybdenum. Columbium, molybdenum, and tungsten are easily oxidized at elevated temperatures; but under space operating conditions, the catalyst would not be exposed to oxygen. Rhenium is a high-temperature-resistant metal similar to tungsten and molybdenum, but with the added advantage of increased ductility. Because rhenium and/or rhenium alloy foams have not before been manufactured, they were not pursued under the program. However, they do offer attractive possibilities for future work.

During the contract, the compatibility of candidate metal foam materials was experimentally evaluated with simulated hydrazine exhaust (26% by volume nitrogen, 37% hydrogen, 37% ammonia) and simulated 24% hydrazinium nitrate/76% hydrazine exhaust (23.8% hydrogen, 37.2%

ammonia, 27.7% nitrogen, 11.3% water) at 1,370°C (2,500°F). No changes were observed with tungsten and molybdenum foams. The presumed nitrogen embrittlement of Haynes 25 which occurred during precontractual in-house testing could not be reproduced under these simulated conditions. However, several Hastelloy X samples which accumulated reactor firing times in excess of 3,000 seconds were badly nitrided and embrittled under reactor conditions. Unfortunately, there was no method available to quantitatively determine and compare the degree of nitridation. In spite of nitridation of Haynes 25 not being reproduced in the laboratory tests, it is considered a marginal material for a metal substrate. Haynes 25 will nitride under the reactor operating conditions, and the small ligament size of the foam makes it susceptible to degradation. A sample of tantalum foil exposed to synthetic hydrazine exhaust became badly hydrogen embrittled and crumbled away to a gray powder within seconds.

2.1.4 Thermal Conductivity

Another evaluation criterion is thermal conductivity. Thermal conductivity is presumed to be of importance for both catalytic and thermal bed applications. In contrast to conventional catalyst beds where particles are in only loose contact with each other, the foam provides an unbroken thermal path between the hot decomposition zone and the injector area, where heat is needed for fast vaporization of injected liquid propellant. Thermal conductivities of a number of candidate materials are listed in Table 2-2 in the order of decreasing conductivity. Next to copper, which cannot be used because of its low melting point, tungsten is the preferred material with respect to high thermal conductivity.

Table 2-2
THERMAL CONDUCTIVITY AND HEAT CAPACITY OF CANDIDATE FOAM MATERIALS

	Thermal Conductivity		Heat Capacity at 294°K	Volume-Specific Heat Capacity
	cal/cm sec°K	at °K	cal/g°K	cal/cm^3 °K
Copper	0.93	293	0.092	0.819
Tungsten	0.40	373	0.034	0.656
Molybdenum	0.35	373	0.065	0.663
Rhodium	0.21	373	0.058	0.722
Platinum	0.17	373	0.032	0.686
Cobalt	0.15	293	0.091	0.810
Nickel	0.15	293	0.109	0.965
Iridium	0.14	373	0.032	0.717
Niobium (Columbium)	0.13	373	0.064	
Haynes-25	0.05	973	0.09	0.823
Hastelloy-X	0.05	863	0.10	0.823
Titanium	0.04	298	0.124	0.558
Zirconium	0.04	373	0.067	0.431
Aluminum Oxide	0.01	1173	0.19	
Zirconium Oxide	0.002	293	0.13	

2.1.5 Heat Capacity

The heat capacity of a catalyst should be as small as possible to allow rapid temperature increase in the bed at the start of operation, resulting in a short response time. This characteristic is particularly important for pulse-mode operation. Heat capacities of candidate materials are listed in Table 2-2 along with thermal conductivity. The major criterion for overall bed thermal response is the product of heat capacity and bed density. This product is also shown in Table 2-2. The heat capacity of tungsten is very low, and its product of heat capacity and density is also the lowest of prime candidate materials for the foam substrate.

2.1.6 Thermal Expansion

The reactor and the catalyst are exposed to rapid temperature changes during operation. Thermal stresses are induced in materials with large coefficients of thermal expansion. The coefficient of thermal expansion of a candidate catalyst material should be low and, in addition to this, should be closely matched with that of the ceramic coating (aluminum oxide) applied. In this manner, differential expansion effects during engine heatup are minimized. As shown in Table 2-3, tungsten satisfies this requirement.

Table 2-3
COEFFICIENT OF THERMAL EXPANSION

Material	Average Coefficient of Thermal Expansion Between 343°K and 793°K $1/^{\circ}K \times 10^{6}$
Copper	17.6
Haynes 25	17.0
Hastelloy-X	16.2
Nickel – 200	13.4
α – Cobalt	12.1
Titanium	9.2
Aluminum oxide	7.8
Tungsten	6.7
Zirconium dioxide	5.5
Molybdenum	4.9
Graphite	3.6

2.1.7 Mechanical Properties

Additional mechanical properties determined include the linear coefficient of thermal expansion, crushing strength, pressure drop, and pore size.

During the program, experimental measurements were made of the linear coefficient of thermal expansion for two cylindrical foam samples, 12.7-millimeter (0.5-inch) diameter by 19.9-millimeter

(0.785-inch) length. One sample was a tungsten (lot number 32-144, 500 μm = 20 mil pore size, sample number 7), and the other sample was a Hastelloy X foam (lot number 32-171, 500 μm = 20 mil pore size, sample number 6A). The coefficient of expansion of the tungsten sample was 8.5 x 10^{-6} 1/^{o}K (4.7 x 10^{-6} 1/^{o}F) which compares well with the literature value of 6.7 x 10^{-6} 1/^{o}K for bulk tungsten. The value for Hastelloy X, 13.5 x 10^{-6} 1/^{o}K is in close agreement with the literature data (13.8 x 10^{-6} 1/^{o}K) (Reference 1). The accuracy on above results is ±10%. It was limited by the rough surface and the short length of the samples. In addition to this, the thermal expansion of tungsten is very small to start with, thus giving only a barely measurable effect

Analytical considerations performed at RRC on other work have shown that a foam material has a coefficient of thermal expansion exactly the same as that of its basic material. This was again confirmed by the above measurements.

2.1.8 Pressure Drop

Pressure drop and crush strength are closely related with percent density and pore size of the metal foam. High-density materials have high crush strength, but the pressure drop is usually intolerably high. The pressure drop of various density samples is shown in Figure 2-6 as a function of flow rate. As can be seen from this chart, pressure drop increases with density of foam samples.

Throughout the multistep preparation of monolithic catalyst beds, the pressure drop was monitored to ensure that none of the samples was inadvertently plugged. A typical pressure drop history of a sample as it underwent the various steps of ceramic coating, and active metal deposition, is illustrated in Figure 2-7.

Pressure drop versus flow rate relationships in capillary tubes may also be illustrated in a nondimensional fashion by plotting a pressure loss modulus N_{PL} versus the effective Reynolds number N_{Re}. In future reports, use of a similar nondimensional presentation will be attempted for pressure drop in foam samples as well. However, the flow through a three-dimensional foam sample is expected to behave differently from the flow through a bundle of capillary tubes. Thus, additional parameters may have to be introduced.

2.1.9 Crushing Strength

The crushing strength of monolithic and granular catalyst samples was determined in a hydraulic press assembly by stepwise increasing the load and simultaneously measuring the compression of the sample with dial gauges. Samples were usually cylindrical in shape and the load was applied in axial direction. Samples with different cross-sections had to be corrected for the different area to which the crushing load was applied.

The crushing behavior of monolithic samples is different from granular materials. The initial deformation at low loads is mainly caused by breakage of single ligaments protruding from each end of the sample. This end effect is more pronounced with large cell size foam where only few ligaments per unit area exist (Figure 2-8).

PRESSURE DROP CHARACTERISTICS OF TUNGSTEN FOAM SAMPLES

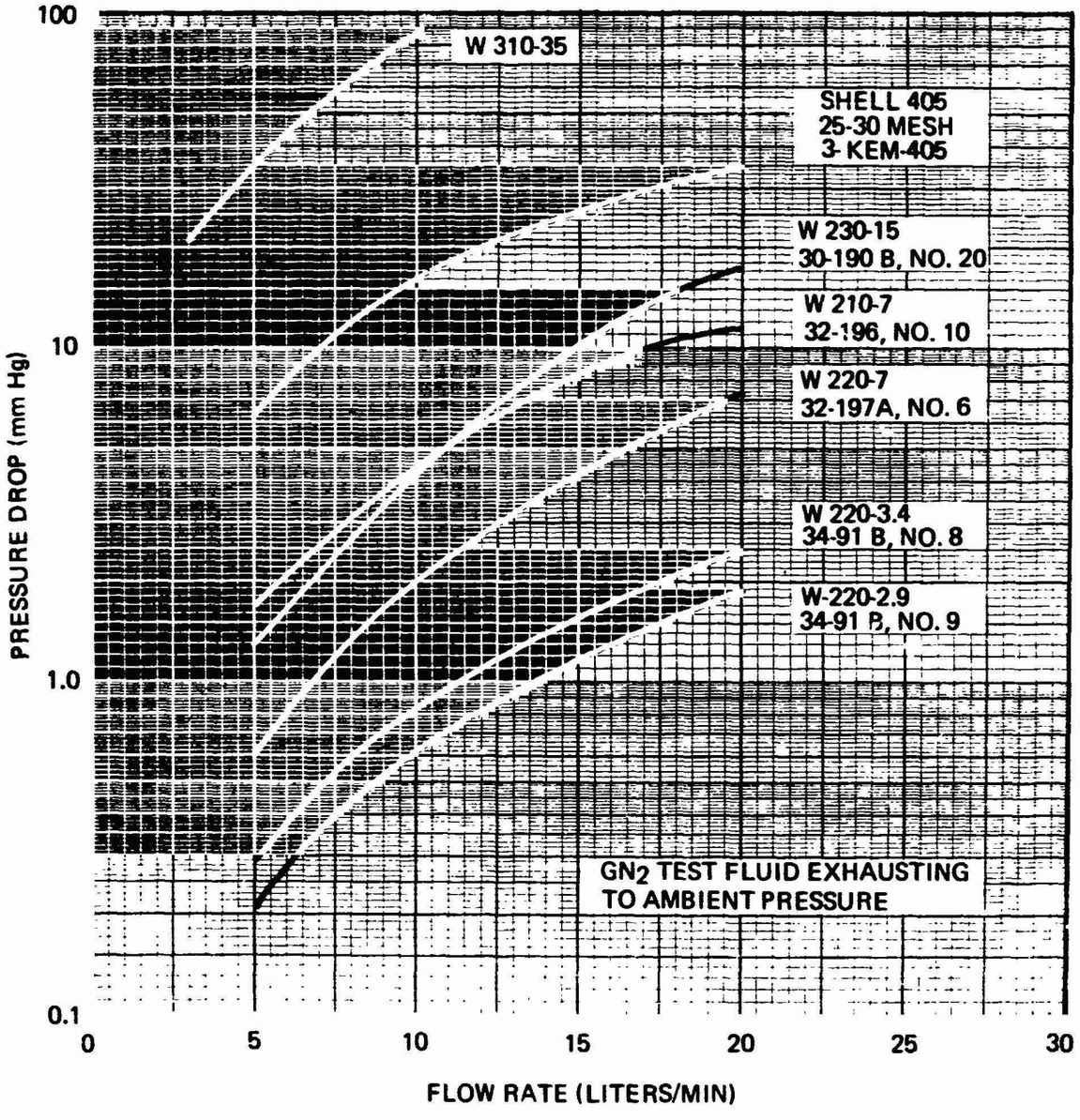

PRESSURE DROP OF A MONOLITHIC CATALYST SAMPLE AT VARIOUS STAGES OF TESTING

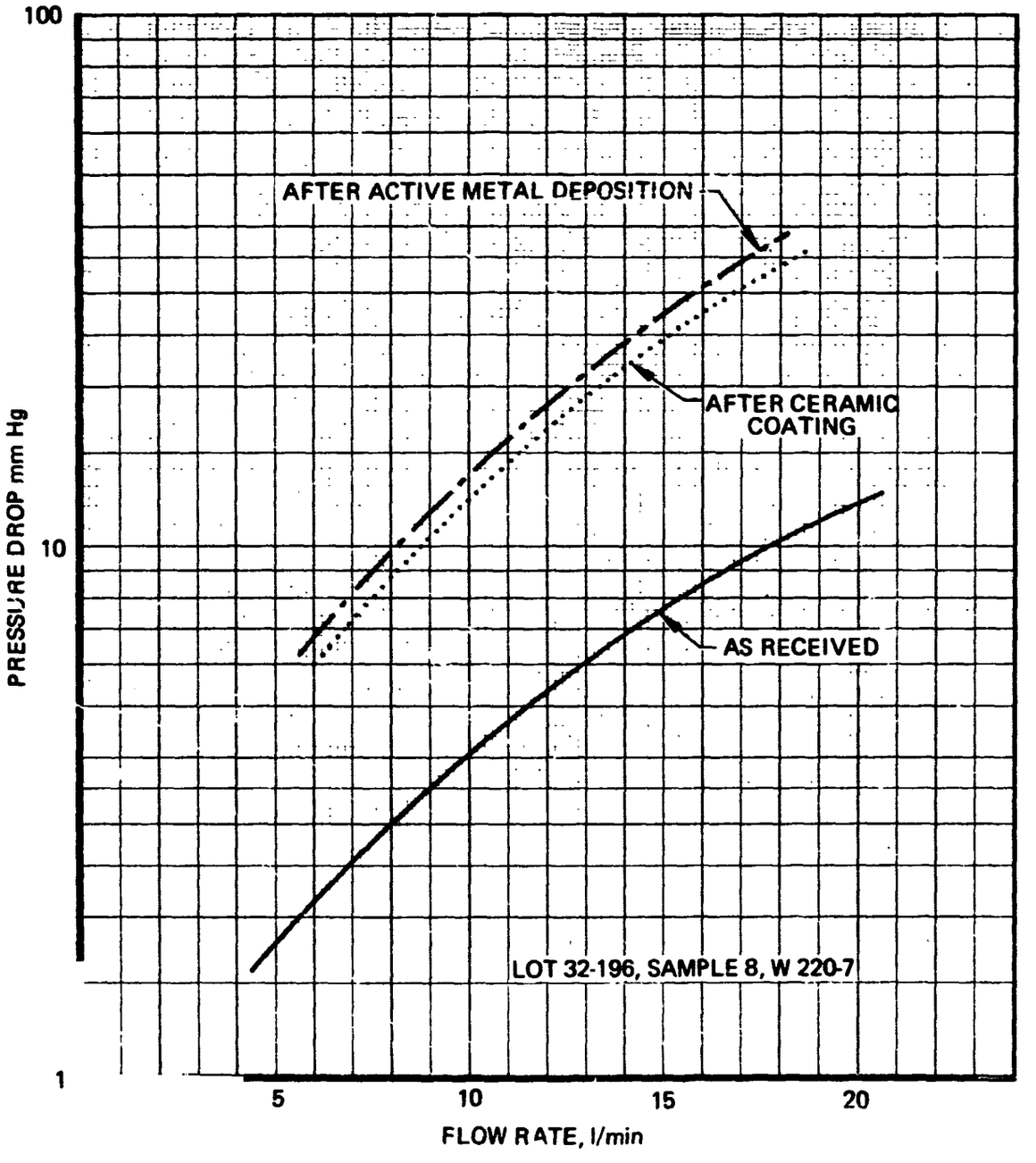

CRUSHING STRENGTH OF FOAM CATALYST MATERIALS

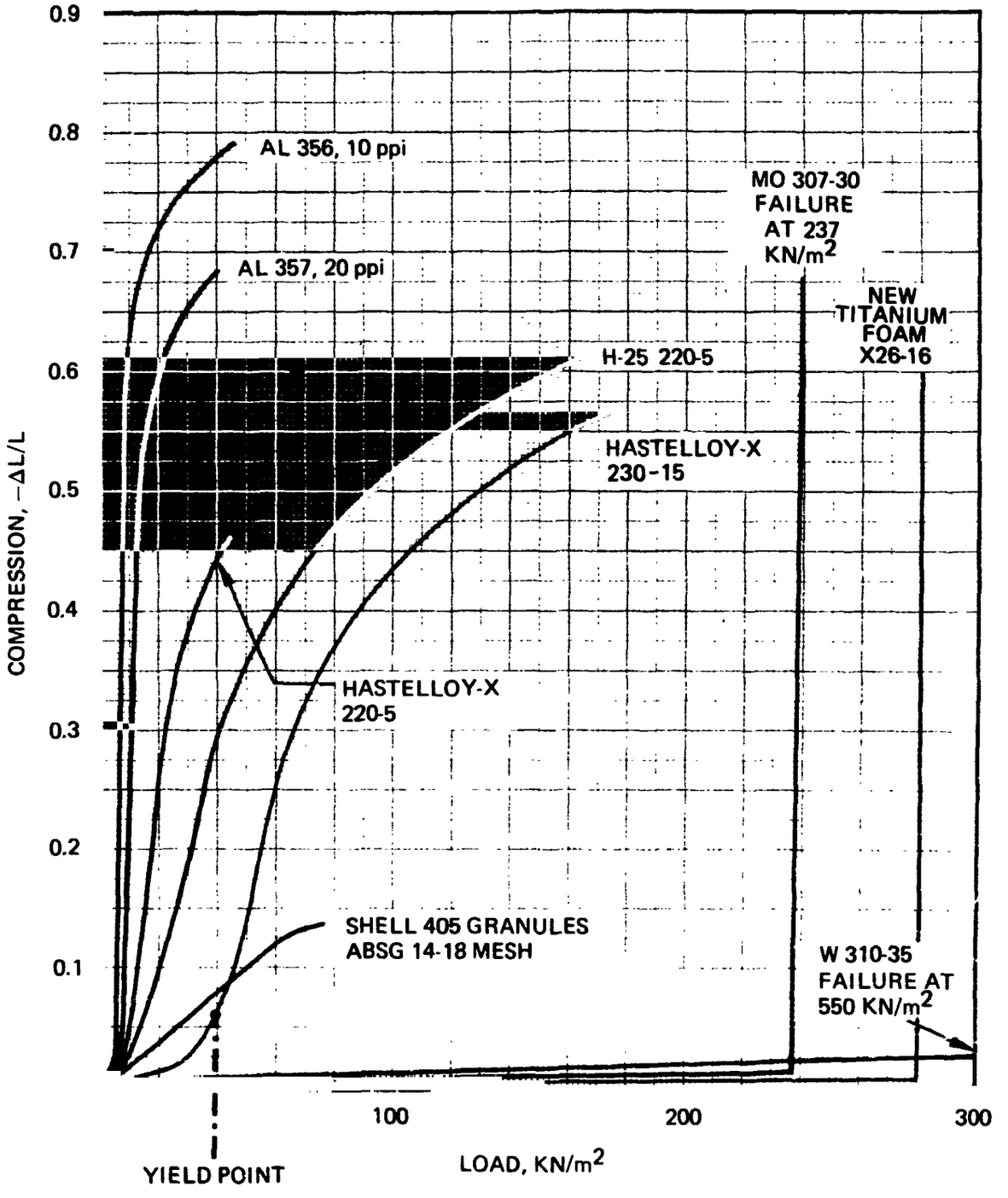

Once the yield point of the foam matrix is reached, a different behavior of ductile (Hastelloy X) and brittle refractory metals (tungsten, molybdenum) can be observed. Ductile metals compress almost linearly over an intermediate range of loads; then a new resistance level is reached when the sample is compacted. Brittle materials, on the contrary, yield at a certain load and the $\Delta L/L$ suddenly increases to approximately 1.

The crushing strength of granular Shell 405 ABSG was determined for comparison. The percent survival at a load of 66.7 kN/m^2 applied was only 32.

Crushing strength of currently used foam materials is lower than granular Shell 405 ABSG. However, the mechanical damage at low loads is less significant than with granular catalyst where a void is immediately formed in the bed. Crushing strength of commercially available refractory foam metals (Figure 2-9) was considerably improved during the monolithic catalyst program. Some higher density foam materials have crushing strengths superior to granular catalyst up to 500 kN/m^2, but these foams also have a higher pressure drop. A high crushing strength is desirable for good handling characteristics. However, it is not the most important parameter in foam selection.

All crushing strength tests were so far performed on bare metal foam samples only. Additional tests will be required to determine if the ceramic coating results in any additional reinforcement to the foam structure.

2.1.10 Chemical Composition

The foam metal which serves as a matrix for monolithic catalysts must be free from contaminants which could vaporize and act as a catalyst poison under reactor operating conditions. With the currently used materials which were sintered under high vacuum at 2,478°K (4,000°F), this problem potential does not exist, because all volatile constituents would vaporize under the conditions of foam manufacture. Two foam samples were analyzed for possible contaminants but none were found. The analysis results are shown in Table 2-4.

2.1.11 Optimum Metal Foam Material

Using the properties of foam metal previously discussed as a basis, RRC selected tungsten as best satisfying the characteristics desired of a metal foam support. This selection is based primarily upon its relatively low heat capacity value and its inertness to the decomposition environment. Because of problems throughout the major part of the program in obtaining tungsten foam of satisfactory structural characteristics, Hastelloy X foam material was used for a majority of the parametric evaluation tests described in Section 4.0.

2.2 CERAMIC COATINGS

Prior to contract award, initial tests of the monolithic catalyst approach were conducted with the active metal deposited directly on the foam substratum. When these tests showed low catalyst activity, further tests were performed with a high active surface area material deposited. The prime candidate for this ceramic coating was aluminum oxide, because it maintains high surface area up to

CRUSHING STRENGTH OF CURRENTLY AVAILABLE METAL FOAM IN COMPARISON TO GRANULAR SHELL 405

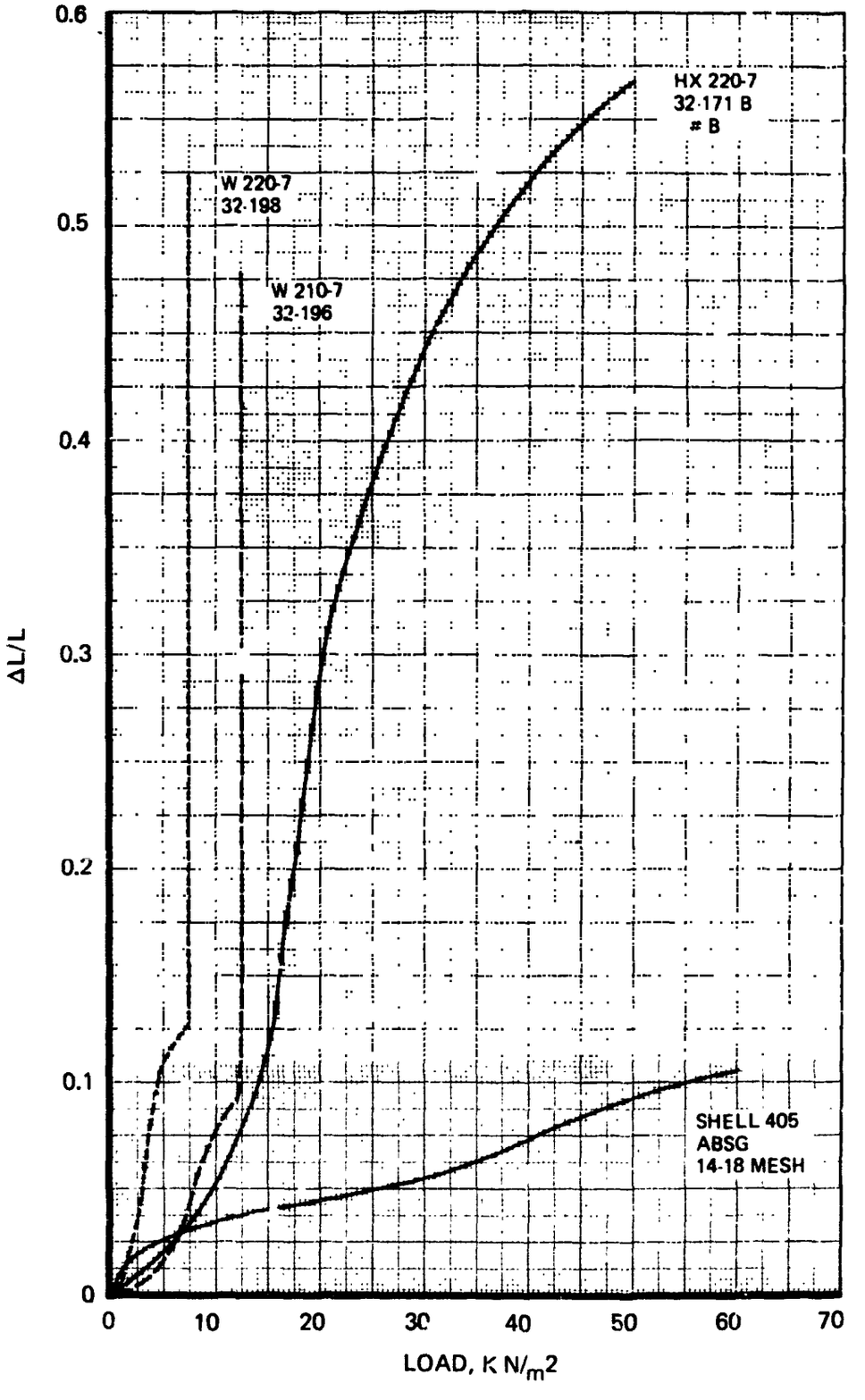

Table 2-4
ANALYSIS OF FOAM METAL SAMPLES

Sample	Element	Found, %	Nominal, %
HX 32-171 A	Al	0.12	
	Ca	0.02	
	Co	2.5	0.5 - 2.5
	Cr	22.7	20.5 - 23.0
	Cu	0.75	
	Fe	18.7	17.0 - 20.0
	Mg	0.01	
	Mn	0.02	1.0 max.
	Mo	5.4	8 to 10
	Si	0.2	1.0 max.
	Sn	0.1	
	W	2.0	0.2 to 1.0
	Ni	balance	balance
W 32-144	Al	0.02	
	Cu	0.001	
	Fe	0.005	
	Mg	0.001	
	Ni	0.05	
	Si	0.03	
	W	balance	99% min.

very high temperatures. Sufficient experience with aluminum oxide as a catalyst carrier was available to extrapolate to its use in monolithic catalysts. As with granular and pelletized catalyst, undesirable shrinkage and subsequent flaking of ceramic coating due to phase changes have to be considered.

Initial catalysts evaluated during the program involved coating the foam metal with a thin layer of Baymal (R), an aluminum oxide sol. Initial tests with catalysts which were prepared with this material revealed a problem of the aluminum oxide flaking off the metal surface after repeated thermal cycles. This coating had been applied after foam metal manufacture by Astro-Met Associates, Incorporated. Several months into the program it was learned that Baymal would no longer be available on the market. This problem, along with the coating adherence problem, led to a redirection of the program to include an in-house development of suitable high surface area coatings and a method of application which would result in satisfactory adherence to the metal foam. This coating study program was initiated and resulted in a silica-stabilized aluminum oxide coating with high surface area (150 to 200 m^2/g). The coating was sintered in place prior to deposition of active metal.

The following parameters are of importance in evaluating ceramic coatings:

a. Adherence
b. Active surface area
c. Sintering characteristics
d. Chemical composition.

2.2.1 Adherence and Surface Preparation

The adherence of a ceramic coating greatly depends on surface characteristics of the foam ligaments on which it is deposited. The adherence is assisted by a porous surface of high roughness characteristics. On the other hand, smooth surfaces were very hard to coat and excessive loss of active material was noted in some test firings. As will be described in subsequent sections, coating adherence represented one of the major problems encountered in the program.

2.2.2 Adherence and Strength of Ceramic Coating

The adherence of a ceramic coating to the metal matrix was tested by vibrating a sample prior to and after subjecting it to 10 temperature shock cycles and then determining the weight loss. The temperature in these shock cycles was 1,253°K (1,800°F) to ambient temperature. However, in most tests the weight change due to loss and adsorption of water from the ceramic was more pronounced than any measurable thermal shock effect.

The adherence of the ceramic coating can be improved by an increase of the sintering temperature. However, a compromise has to be made between increased sintering temperature and loss of active surface area. A considerable portion of the ceramic active surface area is lost while it is being baked in place. The active surface area is a prerequisite for an active catalyst and has to be carefully monitored if the sintering temperature has to be increased. In the course of the program, the sintering temperature was actually increased from 873 to 973°K with only moderate loss in active surface area (see Table 2-5).

Another method to evaluate ceramic coatings was to cast 1/8- by 1/8-inch cylindrical pellets and subject them to the same calcining conditions as those to which ceramic coating would be subjected. Pellets were then tested in a Stokes hardness tester for crushing strength and compared to commercially available pellets such as Harshaw Al 1404. The crushing strength of pellets made from RRC ceramic coating slip, but sintered at 1,253°K for 1 hour, was in some instances superior to that of Al 1404.

2.2.3 Active Surface Area

As revealed by past experience with Shell 405 catalyst, active surface area is a prerequisite to successful catalyst operation. Active surface area is usually determined by nitrogen or krypton adsorption on a degassed surface. The relation between the amount of adsorbed gas and the surface area occupied by it in a monolayer of adsorbed molecules is described by the Brunauer-Emmet-Teller (BET) equation. For this reason, active surface area is frequently referred to as BET active surface area.

Table 2-5
BET ACTIVE SURFACE AREA OF MONOLITHIC CATALYSTS AND CERAMIC MATERIALS

Sample Designation	Calcining Temp., °C	Ceramic Coating, % by Wgt.	Active Surface Area		Loss on Outgassing, % by Weight of Total Sample
			m^2/g Total Sample	m^2/g Ceramic Only	
Ceramic Materials					
Harshaw Al-1404	400	100	138	138	6.9
Reynolds RA1	400	100	241	241	6.7
RA1/Ludox SM	400	100	211	211	
Ampor Alox 100-50	> 2000	100	0.31	0.31	
Ampor Alox 350-20	> 2000	100	0.12	0.12	
Ampor Alox 220-3	> 2000	100	0.22	0.22	
Ceramic Coatings Deposited by Astromet					
Mo 220-7, #Mo6	< 600	17	41.6	245	3.6
W 220-7, #W 12	< 600	(7.5)	4.5	60	0.16
W 230-15, #32-75 F	< 600	3.4	5.8	170	0.28
HX 230-15, #32-76 A	< 600	7.0	14.9	213	0.77
Ceramic Coatings Deposited by RRC					
HX 32-171, #9A	600	28.3	58.6	204	2.42
HX 32-171, #5A	700	27.2	46.4	173	2.04

In the composite structure composed of metal foam and ceramic coating, all BET surface area is contributed by the ceramic coating. The foam by itself has virtually no measurable BET surface area. Also, some aluminum oxide ceramic foams had only very low surface area because of very high sintering temperatures used in the manufacturing process.

Active surface area was measured for a number of ceramic coated monolithic catalyst samples prior to deposition of active metal. The subsequent deposition of active metal decreases the active surface area further; and for this reason, surface area of promoted samples is of no significance in evaluating various ceramic coatings. As shown in Table 2-5, active surface area can be reported for the total sample or for the ceramic coating fraction only. The percent ceramic in the coated sample must be known to relate the two numbers. For the evaluation of ceramic coatings, the surface area based on coating material only is the best parameter, because the percent ceramic in monolithic samples varies with the method of deposition and the foam metal used.

The sintering characteristics of a ceramic determine the loss of active surface area at high temperatures such as those encountered in reactor operation. A good catalyst should retain most of its active surface area under reactor operating conditions. Numerous additives to alumina were tested in an effort to stabilize its structure and prevent surface area degradation. For instance, the pelletized alumina carrier Harshaw Al 1602 is doped with 6% SiC_2 and said to be more stable than the all-alumina carrier Al 1404 This composition is similar to the ceramic coating now used by RRC.

2.2.4 Chemical Composition

The best performing ceramic coating tested during the monolithic catalyst contract consisted of submicron size alumina (Reynolds RA-1) with a silica (du Pont Ludox SM) binder. The nominal dry composition of the coating is 94.5% Al_2O_3, 5.5% SiO_2. Both the alumina and the silica colloid dispersion contain contaminants which may not exceed certain levels to ensure repeatable and successful catalyst operation. Sodium and fluoride catalyze the gamma-to-alpha phase transition of alumina with subsequent loss of active surface area at high temperatures. Sulfate and sulfide are liable to poison the active sites of a catalyst. Typical compositions of the ingredients for the ceramic coating are listed in Table 2-6. Tolerable upper limits for contaminants were not yet established, but satisfactory results were achieved with these commercial grade chemicals. The coating procedure is described in paragraph 3.4 along with the active metal deposition.

2.3 ACTIVE METAL DEPOSITION

(This paragraph is contained in a separately bound, classified addendum to this report.)

2.4 EVALUATION OF CATALYST SAMPLES

During the development phase when various catalyst supports and methods of promoting the catalysts were screened, spot plate activity and ignition delay tests and hydrogen chemisorption were used to evaluate finished catalysts before more costly reactor firings were made.

Table 2-6
CERAMIC COATING INGREDIENT COMPOSITION

Ingredient	Composition	% By Weight
Alumina RA-1	Al_2O_3	91.5
	Na_2O	0.5
	SiO_2	0.1
	Fe_2O_3	0.02
	TiO_2	0.002
	H_2O	balance
Ludox SM	SiO_2	15
	Na_2O	0.1
	NaCl	0.001
	Na_2SO_4	0.003
	H_2O	balance

2.4.1 Spot Plate Activity Tests

Preliminary evaluation of catalyst activity was performed by dropping some drops of hydrazine on a catalyst sample sitting on a ceramic spot plate in air. Results from these tests must be interpreted with caution, because of a twofold effect of atmospheric oxygen. First, the presence of active oxygen on the catalyst surface makes the catalyst appear more active than it actually is. Second, the hot catalyst may be damaged by exposure to air after the test. In order to avoid this, in succeeding tests the catalyst was placed in a test tube with a nitrogen purge and sealed with a fiber glass ball. The nitrogen purge was maintained between tests in order to prevent air from affecting the activity of the catalyst sample. Early catalyst samples, where iridium was deposited directly on Haynes 25 foam without the intermediate deposition of an active surface area coating, showed a high initial activity when tested in air, but a very low activity after the first test under nitrogen. These samples were active under nitrogen only during the first test when they were still loaded with active oxygen. The active oxygen was then rapidly removed by reaction with hydrazine.

Results from spot plate activity tests are summarized in Table 2-7.

2.4.2 Evaluation of Spontaneity

The spontaneity of catalyst samples was tested with a versatile laboratory tool, the RRC ignition delay tester. With this instrument, the delay between the contact of propellant with the catalyst and the first exotherm can be measured.

2.4.2.1 Definition of Ignition Delay

The ignition delay of monopropellant reactors is a very important evaluation criterion where short response times are required (attitude control, trajectory correction, orbit insertion). For the data

Table 2-7
SPOT PLATE ACTIVITY TESTS

Sample	Atmosphere	Results
6.5% Ir on Haynes-25 foam 220-7 without prior Al_2O_3 coating	Air	Repeatedly active.
Same	Nitrogen	Active with first test only, floods out with hydrazine at consecutive tests.
7% Ir on aluminum oxide foam 260-3	Air	Very slow ignition. More active when glowing red hot from previous decomposition.
5% Ir on Haynes-25 220-7 with Al_2O_3 coating	Air	Repeatedly active.
Same	Nitrogen	Repeatedly active.

compared herein, ignition delay is defined as time lapse between valve open signal and 1% of steady-state chamber pressure. Unfortunately, this delay is composed of a mechanical delay (valve opening time, time for propellant flow to reach catalyst) and a chemical delay. The mechanical delay is not always constant and may vary with test conditions. It is not possible on the basis of reactor firing data alone to differentiate between mechanical and chemical delay. The ignition delay tester used in this study measures the chemical delay only. This method has proven to be valuable in studying the effects of numerous variables (catalyst activity, catalyst pretreatment, catalyst poisons, adsorbed gases, temperature, pressure) on the ignition delay. With this improved system, not only an exotherm as such, but also the magnitude of an exotherm and the rate of temperature increase could be used in defining the ignition delay.

A reasonably good correlation of ignition delay data (obtained with the prototype system) with those reported by Shell Development Company was obtained when both data were plotted together on the same sheet (Figure 2-11). This confirms that both methods basically measure the same phenomenon, although the scatter of data points is considerable. The line of proportionality does not intersect at zero, because data reported by Shell on their catalyst specification sheets include a mechanical delay.

2.4.2.2 Description of Apparatus

The central part of the ignition delay test apparatus is a ceramic or quartz crucible which holds the catalyst sample and rests on a sensitive piezoelectric crystal microphone. The microphone picks up

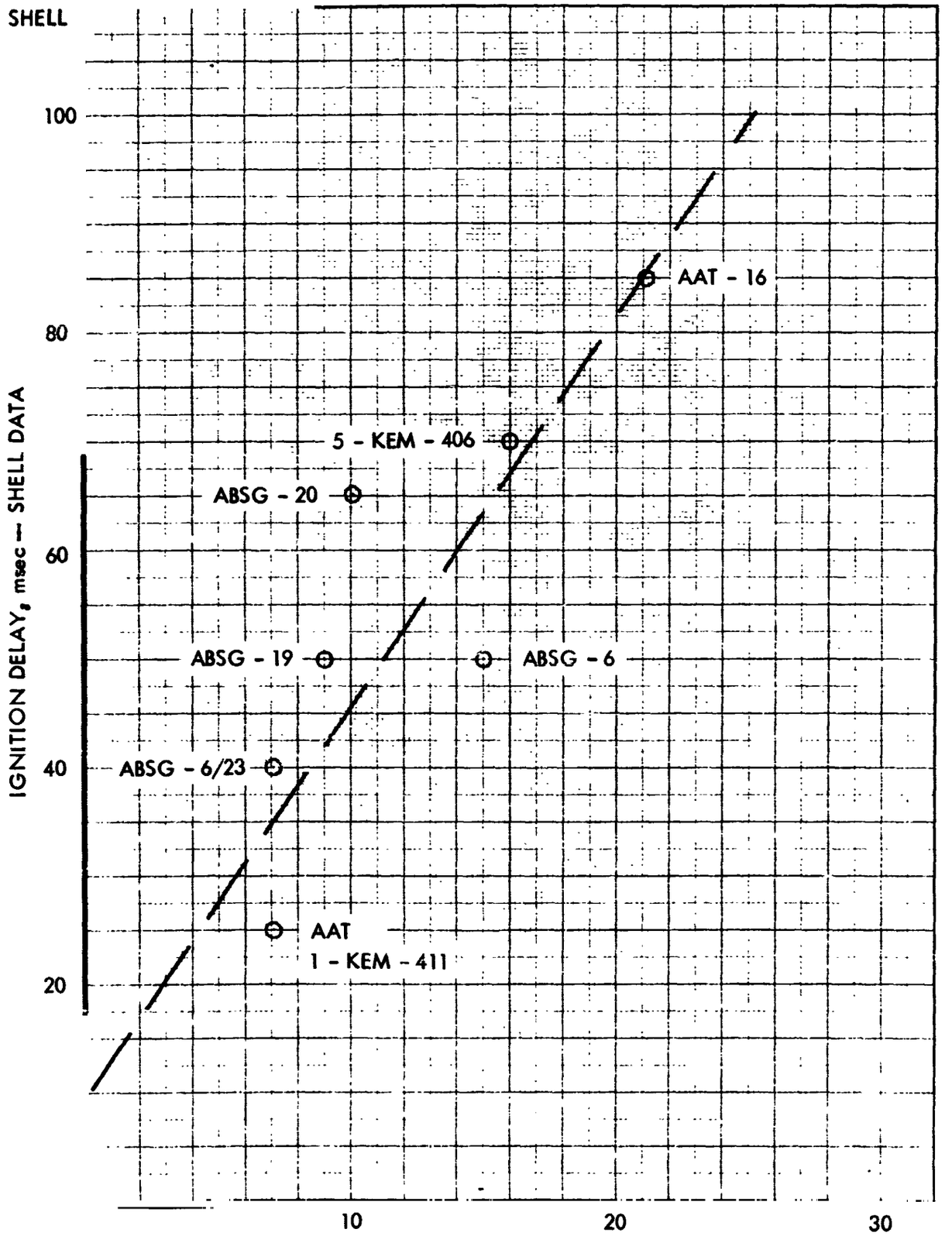

CORRELATION OF IGNITION DELAY DATA, SHELL VS RRC

the momentum of propellant impact when it hits the catalyst surface. The reaction noise is recorded on the same oscillograph trace. The crucible and the microphone are mounted in a temperature conditioned beaker. A thermopile arrangement was so sensitive that even the heat of wetting of the bare carrier material, Harshaw 1404 or Reynolds RA-1, could be recorded, although it was several orders of magnitude smaller than the heat evolved during hydrazine decomposition on active catalyst.

Unshielded thermocouples gave the fastest response because of the small heat capacity of the welded joint bead. Even better response was expected by the use of surface thermocouples where the thickness of the hot junction has been decreased by grinding down to 0.001 inch. However, it was not possible to use a thermopile arrangement with the metal foam catalyst samples as the electrically conductive foam shorted the thermopile output. Insulating the thermocouples from the foam sample would have drastically increased the response time. Two calibrated, redundant surface thermocouples were used for metal foam catalyst samples instead. For optimum response, the thermocouples were implanted into the monolithic catalyst sample. A 1.5-millimeter (0.05-inch) diameter hole was drilled radially through the sample to hold one thermocouple on each side.

Early ignition delay tests used a photo cell to signal the propellant flow on the catalyst. The drop of propellant crossing the focused light beam caused an interruption of a lightmeter trace on the oscillograph. However, the light beam technique was abandoned with later tests because it did not give reproducible results. The microphone method is considered to be the most reliable method for determining the propellant/catalyst contact time.

Both the microphone and the thermocouple or thermopile outputs were recorded on a Honeywell Visicorder high-speed oscillograph operating at a speed of 20 in./sec with a timing of 10 milliseconds. The best obtainable time resolution was 2 milliseconds (estimated).

With the currently used ignition delay tester, the propellant was injected from a temperature-conditioned feed line through an Eckel micro valve. The micro valve was operated via a variable micropulser which allowed pulse widths as low as 10 milliseconds. At 25-psig feed pressure, a 60-millisecond pulse resulted in the ejection of 0.3 milliliter hydrazine per pulse. The use of a valve instead of a pipette enabled the ignition delay tester to operate under vacuum conditions as well. The holdup volume of the downstream end of the valve was extremely small. For best results, the valve and the injector were placed as close to the catalyst sample as possible.

Initial tests were performed with a 1.27-centimeter (0.5-inch) outside diameter showerhead injector plate to achieve good propellant dispersion. However, the dispersed propellant jet would not penetrate deep enough into the foam metal sample to give uniform reaction over the entire volume. Reaction appeared to be restricted to the upper portion of the catalyst sample because of its unconfined position in the crucible. The showerhead injector plate was then removed and the undispersed propellant jet was allowed to impinge on the sample, resulting in improved penetration and shorter ignition delays. Penetration was essential because the thermocouples were located in the center of the sample, not on its upper surface. No pressure measurements were taken because the catalyst sample is relatively unconfined and the quartz crucible will not withstand high pressures.

The propellant feed system was designed such that no materials other than stainless steel or teflon are in contact with the hydrazine propellant. It consisted of a 75-milliliter Hoke cylinder as propellant reservoir with a pressure gauge, a 100-psig relief valve, a nitrogen pressurization valve, a propellant enable valve, the temperature conditioning jacket, a propellant filter, and the propellant micro valve. The propellant and the catalyst thermal conditioning jackets were connected to a constant temperature circulator by which the temperature could be varied between 255.2°K (0°F) and 344°K (+160°F). All testing was performed at 298°K (77°F), and the calibrated thermocouples in contact with the catalyst were used to monitor the initial catalyst temperature before each test.

The ignition delay system was contained in a T-shaped vacuum vessel with O-ring sealed flanges, which provided excellent accessibility to the system from all sides. A schematic of a modified version of this system is shown in Figure 2-12. This version will allow the catalyst to be preheated in a vacuum to obtain a clean catalyst surface. Up to this time, the microphone and quartz crucible were rigidly mounted and could not be moved for preheating the catalyst under vacuum.

The T-shaped vacuum vessel could be alternately evacuated and filled with inert gas, argon, or nitrogen. All ignition delay tests were performed under argon. The argon was passed through a cartridge with hydrogen-loaded Shell 405 catalyst which served as an oxygen scavenger to remove last traces of oxygen from the inert gas. Oxygen present as a trace contaminant (10 ppm) had a very pronounced effect on measured ignition delays.

A photo of the ignition delay setup with the associated equipment is shown in Figure 2-13. The photo shows (from right to left) the vacuum line with mercury diffusion pump and McLeod gauge, the constant temperature water circulator, the ignition delay tester with propellant feed system mounted on the flange, a power supply for the valve, and the instrumentation rack with oscillograph, amplifier and micropulser.

2.4.2.3 Ignition Delay Test Procedure

Before and after each test, the test specimen was weighed to record eventual weight loss. The specimen was then placed into the quartz crucible, and the thermocouples were inserted into the predrilled holes. The Dewar flask which held the cold junctions was filled with ice and water, and the thermocouple circuit was checked. The top flange with the propellant feed system was then inserted and bolted to the ring flange. Following the evacuation of the system and a leak check, the system was filled with argon. A slow argon purge was maintained during the test. The propellant tank was evacuated, filled with 20 milliliters of hydrazine, and pressurized with 2.7 atmospheres (25 psig) of nitrogen. The temperature conditioning system was set to the desired temperature and actuated at least 20 minutes prior to each test.

The micropulser was set at 60-millisecond single-pulse duration, the oscillograph chart drive was started, and the valve opened for 60 milliseconds. Immediately after the propellant injection, the argon purge was turned off and the system first evacuated with a water aspirator, then with the rotary vacuum pump. A test series consisted of 10 consecutive propellant injections. Between each

IGNITION DELAY TESTER SCHEMATIC, DETAIL

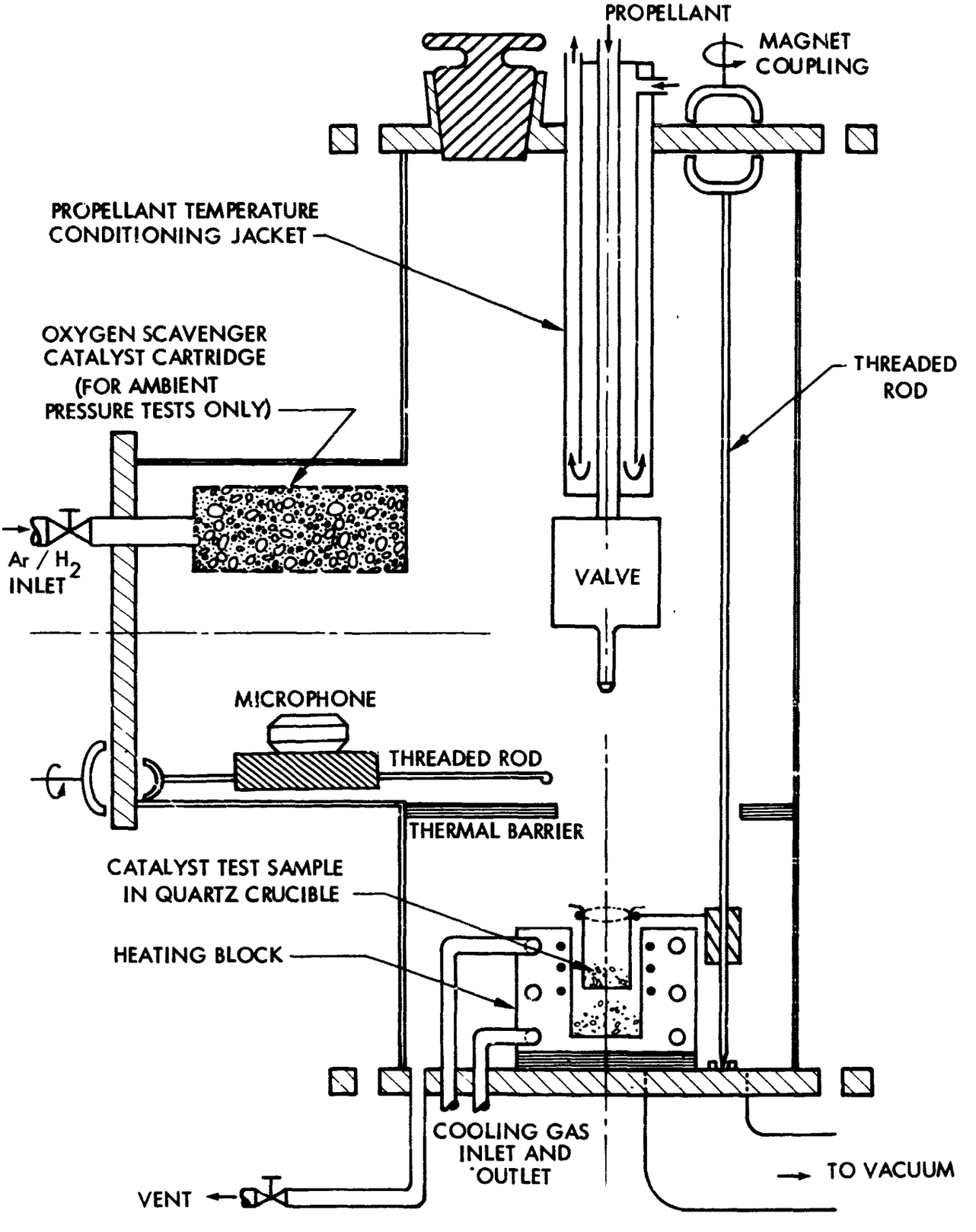

IGNITION DELAY TEST SETUP

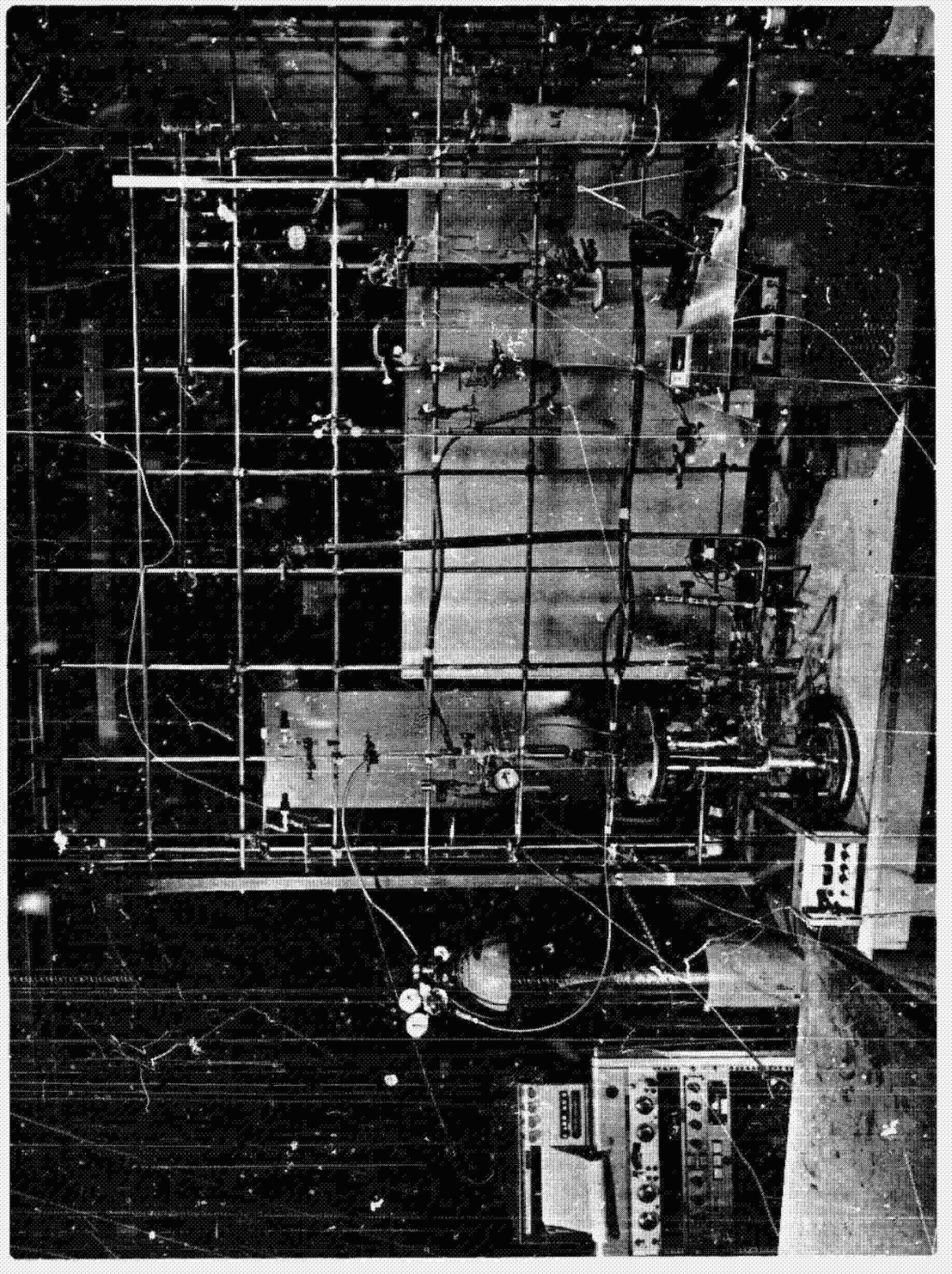

56000-37

Figure 2-13

injection the system was evacuated for 5 minutes to remove decomposition products of the previous injection. Even though the catalyst was still warm at the beginning of the evacuation, the 5-minute evacuation was not sufficient to remove all ammonia from the catalyst. Ammonia adsorption was shown to decrease catalyst activity remarkably (References 2, and 3). It is also reported that ammonia does not readily desorb from the catalyst unless high temperature and vacuum are applied. This technique would be possible with the modified version of the ignition delay tester but is not required for the current test series.

A typical oscillograph record of an ignition delay test is shown in Figure 2-14. The microphone trace not only recorded the impact of the propellant, but also the noise of the subsequent reaction on the catalyst surface. For data reduction, a straightedge was fitted to the linear portion of the thermocouple trace and the intersection with the temperature baseline taken as the first sign of exotherm. With vacuum tests, the cooling due to propellant evaporation could also be recorded and overlaps with the exotherm because of propellant decomposition. The ignition delay was taken as the time between impact of the propellant and the first indication of exotherm.

2.4.2.4 Discussion of Results

A summary of performed ignition delay tests is given in Table 2-8. As a general trend with all samples tested, the ignitic delay increases with increasing numbers of cold starts. This increase is also observed with Shell 405 catalyst and may be attributed to the following effects:

a. Loss of active oxygen after the first reaction with hydrazine
b. Active sites on the catalyst blocked by adsorbed gases (ammonia, hydrogen)
c. Active sites on the catalyst poisoned by propellant contaminants (aniline)
d. Loss of active material.

Some catalysts recover after air is readmitted to the catalyst, causing the adsorbed hydrazine decomposition products and the catalyst surface to become oxidized. During the testing of monolithic catalyst samples, air was occasionally admitted for a last test. However, this did generally not improve catalyst performance. Consequently, the loss of activity must be assumed to be due to mechanical loss of active material.

One of the main purposes of the spontaneity testing was to establish the required active metal concentration. The considerations leading to the selection of the optimum active metal concentration are outlined in Section 4.0. Based on the data listed in Table 2-8, 20% active metal content in Hastelloy X produces more active catalysts than 10%. Hastelloy X and tungsten or molybdenum samples are not comparable on a weight percent basis. Ignition delays with ruthenium were slightly longer than with iridium.

In addition to catalyst properties, ignition delays were also dependent on the method of hydrazine injection. Ignition delays with the otherwise identical samples W3 and W1 improved when omitting the showerhead injector plate and injecting a single jet of propellant only.

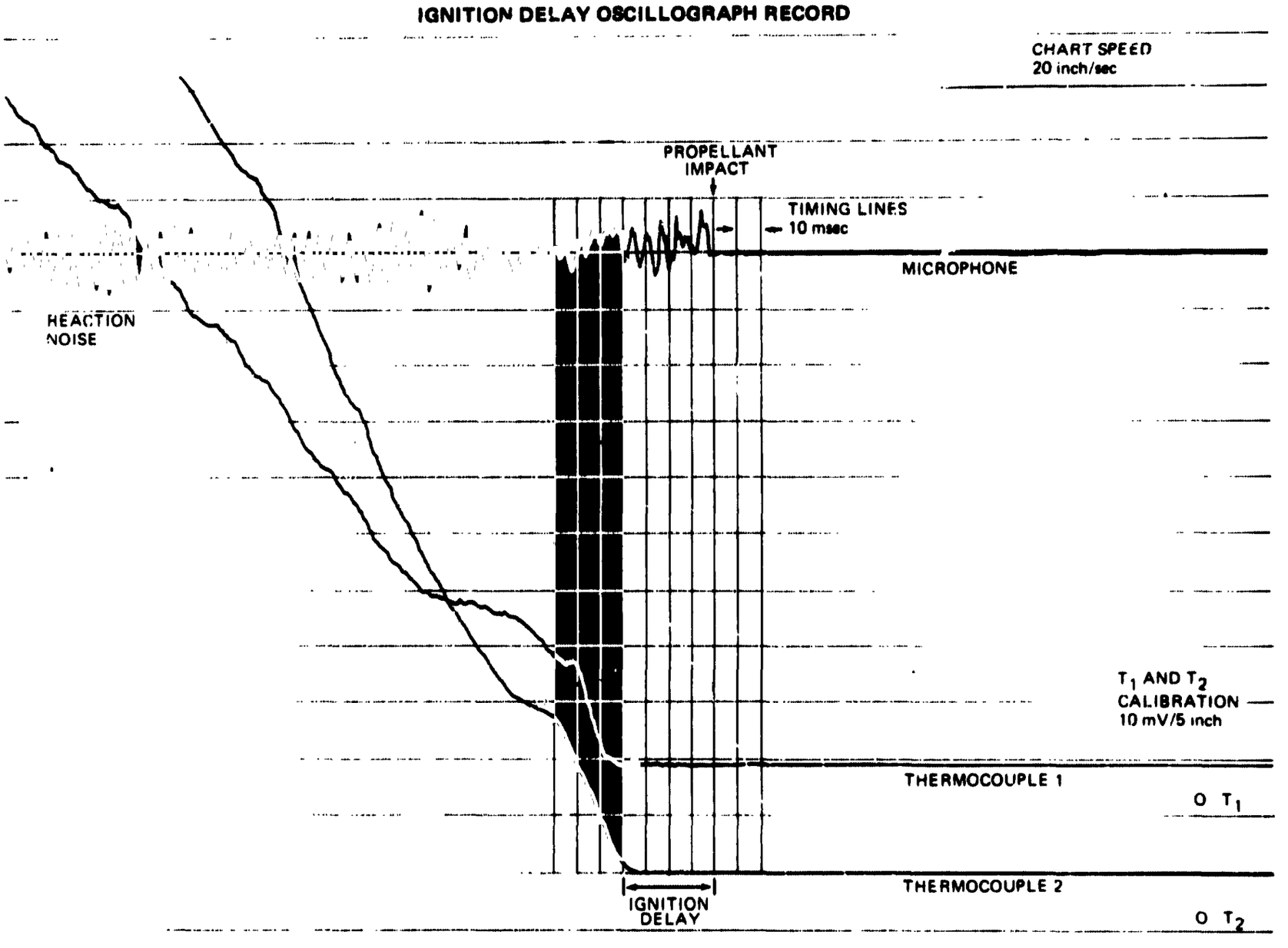
IGNITION DELAY OSCILLOGRAPH RECORD
CHART SPEED
20 inch/sec
PROPELLANT
IMPACT
TIMING LINES
10 msec
MICROPHONE
REACTION
NOISE
T1 AND T2
CALIBRATION
10 mV/5 inch
THERMOCOUPLE 1
O T1
THERMOCOUPLE 2
O T2
IGNITION
DELAY

Figure 2-14

Table 2-8
SUMMARY OF IGNITION DELAY TEST RESULTS

				Ceramic Coating		Iridium		Ignition Delay, msec												
Foam Metal	Type	Lot No.	Sample No.	Type	%††	% by Weight	g/cm³	1	2	3	4	5	6	7	8	9	10	11	Weight Loss %	Remarks
HX		32-22 B1	Ir 2			20.8	0.19	20	35	55	120	110	108	118	135	135	150		5.7	Showerhead injector
HX		32-22 B2	Ir 3	Baymal		5.2	0.07	60	100	220	215	270	420	420					3.2	
HX			Ir 6†	deposited		14.8	0.15	70	90	120	•	•	•	•	•	•	240		9.9	Undispersed jet
HX	220-7	32-22 B3	Ru 5	by		14.3 ruthenium	0.12	65	105	175	230	(150)	310	340	300	300**			3.8	Showerhead injector
HX	220-7	32-22 B2	Ru 7	Astromet		8.7 ruthenium	0.04	50	80	110	235	350	350	210	210	190			3.3	
W		1-20-70	W 1†			2.9	0.05	25	80	120	140	180	180	200	200	260	230	256*	2.6	
W		1-20-70	W 3	Baymal +	Not	2.7	0.07	25	70	130	360	800	1 060	(265)	(300)†				7.4	Undispersed jet
W		1-20-70	W 6	Alon	determined	2.8		190	130	190	430								1.1	Last test with showerhead injector
Mo		1-20-70	Mo 1			5.0		40	240	230	230	460	520**						1.9	
Mo		1-20-70	Mo 4	Baymal		2.5		80	260	340	•	•	•	•	•	•	300		5.7	
Mo		1-20-70	Mo 2	deposited by		1.9		45	90	75***									5.0	
Mo		1-20-70	Mo 7	Astromet		5.0		100	85	120	140	120	•	•		•	180		4.0	
HX		32-76	B			2.2	0.07	260	500	•	•	•	•	•	125**				0.3	
HX	230-15	32-76	1			2.3	0.07	100	680	680	•	•	•	•	180				0.4	
W	230-15	32-75	C	Baymal + RRC	17.6	3.1	0.09	12	•	40	52	65	•	•	•	•	145		0.0	
W		32-75	1	RA 1/Ludox (RRC)	10.4	2.0	0.06	23	25	•	•	100	•	•	•	•	320		3.1	
W	220-7	1-20-70	17	Baymal + RRC	23.2	5.3	0.1	20	40	58	50	80	120	140	160	200	200	185	3.7	
For comparison Shell 405 1/8 x 1/8 pellets		4 KEM-401						18	27	24	(12)	23	23	23	36	30	62			

*Intermediate tests not recorded in order to speed up testing
**After readmission of air into system
***Discontinued due to malfunction of system

†After heating for 1 hour in simulated N_2H_4 exhaust at 980°F
††Before deposition of active metal

It could also be noted that samples which were exposed to simulated hydrazine exhaust for 1 hour at 1,253°K suffered less weight loss than fresh samples. Apparently the adherence of the coating was improved in this treatment. The activity of the samples did not suffer from this treatment.

When going from samples with 7% to samples with 15% density, it was noted that the temperature increase leveled off at approximately 373°K before increasing further. The rate of temperature increase was lower than with 7% density samples. Apparently the large mass of metal foam absorbs a significant fraction of the heat released during the transient phase. Similar phenomena were later observed with the chamber pressure transient of 15% density samples in reactor firings.

2.4.3 Hydrogen Chemisorption

The measurement of hydrogen chemisorption is a very useful tool in evaluating catalyst activity. Hydrogen chemisorption depends on both a high active surface area and the presence of finely dispersed active metal. Bulk active metals show hardly any hydrogen chemisorption.

Hydrogen chemisorption was measured by a thermoconductivity method with 99% argon/1% hydrogen in a gas chromatograph. The samples were degassed at 773°K and then rapidly cooled to 273°K in the Ar/H_2 stream. The recorded peak area was proportional to the adsorbed hydrogen.

The results summarized in Table 2-9 show that hydrogen chemisorption of monolithic catalysts on a total weight basis is lower than for Shell 405 catalyst. This must be expected because most of the monolithic catalyst is metal foam which does not significantly contribute to the surface area. In order to evaluate the active metal deposition, the μ moles hydrogen chemisorbed should be related to the amount of active material, i.e., the active metal plus ceramic only. The numbers thus obtained are in the same order of magnitude as for Shell 405.

Because the hydrogen chemisorption measurement alters the properties of the catalyst, no post-hydrogen chemisorption samples could be used for test firings. Instead, control samples were prepared under exactly identical conditions along with samples intended for reactor firings.

Decrease of hydrogen chemisorption with firing time was measured for two post-firing samples. The decrease is no greater than for Shell 405 catalyst. The record sample with 7,700 seconds accumulated burn time exhibited a reasonably high residual hydrogen chemisorption after the firings.

Table 2-9
HYDROGEN CHEMISORPTION OF MONOLITHIC CATALYSTS AT 273°K

Foam Metal	Type	Lot. No.	Sample No.	Ceramic Coating		Iridium		Hydrogen Chemisorption		Remarks Sample History
				Type	% by Weight	% by Weight Total	% by Weight in Al_2O_3 + Ir	μ Moles/g Total	μ Moles/g Al_2O_3 + Ir	
HX	220-7	32-22 B1	Ir 1	Baymal deposited by Aetromet	Not determined	20.8		41	240	
W	220-7	20-70	W 2			2.5		18		
W	220-7	32-144	1			17.1	6.4	28.7	25	122	Post firing sample
HX	220-7	32-171	3 A			30.7	13.0	32.8	71	181	Coated sample for 32-144 #1 above. Fresh sample
HX	210-7	34-210	5 D	RA-1 Ludox deposited by RRC		39.1	16.5	33.5	45	90	Added NH_3 to active metal solution, pH 9
HX	220-7	32-171	3 B			32.5	16.1	37.1	103	233	Coated sample for W 32-196 #5 and #8. First sample coated from 12.5% Ir solution
HX	220-7	32-171	4 B			35.0	16.0	35.3	48	107	Accidentally overheated when degassing. Number should be higher
W	220-7	32-197 A	1			19.5	9.1	34.0	79.2	102	Post firing sample, 16 firings, 7,700 seconds total burn time
For comparison Shell 405 ABSC						32	32	287	287		

3.0 PREPARATION OF MONOLITHIC CATALYST SAMPLES

The preparation of monolithic catalyst samples is a multistep procedure. It consists of selection and characterization of a foam material, machining it to size, coating with active surface area ceramic, and promoting with active metal. The various steps are best illustrated in Figure 3-1 where monolithic catalyst samples for a 0.5-lbf reactor are shown at various steps in the preparation.

3.1 SELECTION OF FOAM SAMPLES FOR MONOLITHIC CATALYSTS

Rocket Research Corporation Specification MS-0122 was used to control and purchase foam metal under the contract. In addition, as previously described, X-rays are taken of all foam material to observe uniformity, and pressure drop measurements are made to ensure no blockage.

3.2 MACHINING OF FOAM SAMPLES

Foam materials which are received as bulk samples had to be machined by electric discharge (EDM). Tungsten samples had to be filled with a hard wax first and then machined by conventional methods. The wax was then removed by heating to 2,300°K in a vacuum furnace.

3.3 METAL FOAM SURFACE PREPARATION

Throughout the period when nickel, Haynes 25, and Hastelloy X foams were used, foam metals were coated after degreasing and cleaning the samples without further surface preparation. Because these foams usually have a very rough and sometimes porous ligament surface, good adherence of the ceramic coating was achieved. Some adherence problems were encountered with the first tungsten foam samples for reactor firings, which had a very shiny and "too-perfect" surface. One of these samples is shown on Figure 2-2.

Various methods for roughening the surface were tried. Chemical etching was without effect because tungsten is chemically very inert. Controlled oxidation in 1% oxygen/99% argon appeared to weaken the foam structure. Good adherence was finally achieved with samples which had undergone additional treatment at the manufacturer's plant. Tungsten powder was dusted on the surface of the ligaments. During the last furnace cycle, the temperature was raised just enough so the powder would adhere to, but not fuse into, the surface. Good results were obtained with catalysts prepared from these foam samples. Further studies to modify the metal surface prior to deposition of the ceramic coating are warranted in order to improve adherence and catalyst life.

3.4 CERAMIC COATING

The weighed and cleaned foam samples were placed on a petri dish and identified. A ceramic coating slip was made from 13 grams of submicron-size alumina RA-1, 3.5 grams of water, 5 grams of silica colloid Ludox SM, and one drop of a wetting agent. The mixture was thoroughly stirred to remove all lumps. The foam sample was then submerged in the mixture and vacuum was applied

MONOLITHIC CATALYST SAMPLES AT VARIOUS STAGES OF TESTING

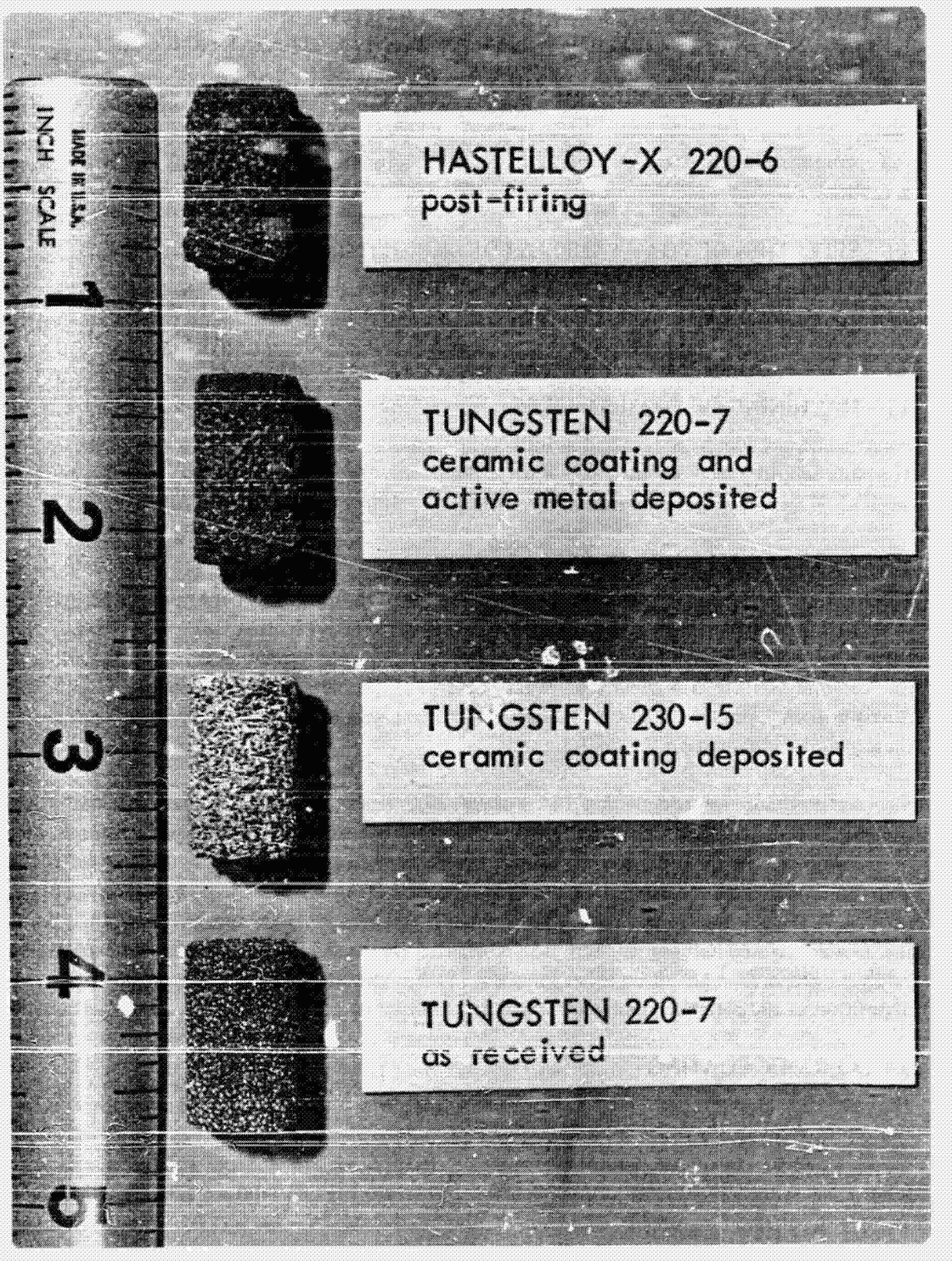

56000-39

Figure 3-1

three times to aid penetration. The sample was then taken out of the mixture, and the excess coating was blown out with moisture-saturated air. The samples were allowed to air dry for at least 3 hours and then dried at 393°K for at least 12 hours. Calcining was achieved by heating them in a quartz tube under hydrogen for 1 hour at 973°K. The samples were allowed to cool off under hydrogen to between 373 and 423°K and finally cool to ambient in a desiccator. The weight gain was determined and the percent ceramic calculated. All samples were then retested for pressure drop, and a new ΔP curve was plotted on the chart accompanying each sample. From this increase in ΔP, it could be determined whether or not an excessive number of pores had been inadvertently plugged with ceramic. A typical ΔP history of a sample is shown in Figure 2-7.

3.5 ACTIVE METAL DEPOSITION

(This paragraph is contained in a separately bound, classified addendum to this report.)

3.6 RANGE OF PARAMETERS STUDIED

In total, 14 parameters can be varied in order to arrive at an optimal monolithic catalyst bed. Obviously not all of these parameters could be included in the original test matrix. This restriction existed not only because of lack of time, but also because the significance of some additional parameters became apparent only during the test program. Table 3-1 shows a summary of the more important parameters.

Initial testing was limited to 20-mil pore-size foam materials. Ten-mil pore-size materials, in particular for refractory metals, were more difficult to manufacture and became available only toward the end of the program as the foam technology advanced. When small pore size foams were being made, the risk of accidentally plugging pores or leaving membranes across windows was higher than with large pore sizes. Small pore sizes were desirable because the fuel entering the bed was more finely dispersed and exposed to more surface area than with coarse foam. This resulted in faster response and smoother reactor operation.

However, as the volume and temperature of the decomposition gases increases, a coarser foam is desirable for the lower portion of the bed to reduce the pressure drop found with 10-mil pore-size foam samples. This is possible by sandwiching or by stacking up samples of different pore sizes in a composite bed.

The density of a foam matrix determines its strength and its weight. Sufficient strength to withstand the reactor environment is certainly a prerequisite. Typical foam densities used varied around 7%. Samples with higher foam densities were very heavy. In addition to that, too much inert material had to be heated up during the start period. This resulted in a long transient, a stepwise chamber pressure increase, and flame front shifts during the early phase of reactor tests. The time to reach 90% P_C was longer than with lower density samples.

The ceramic coating parameter studied was the type of coating and mode of deposition. Adherence was a very important criterion, and improvements are still possible in this particular area. The ceramic loading was limited by the danger of plugging pores and unduly increasing pressure drop of

Table 3-1
RANGE OF PARAMETERS STUDIED FOR
MONOLITHIC CATALYST BED EVALUATION

Parameter	Range	Important For
Foam Parameters		
Pore size	10 mil to 30 mil	Pressure drop, response, P_c roughness
Density	3.5% to 15%	Mechanical strength, response
Type of foam metal	Hastelloy-X, Tungsten, Molybdenum	Exhaust compatibility, strength Catalyst durability
Ceramic Coating		
Active surface area coating	SiO_2, Al_2O_3 composition	Catalyst activity
Sintering temperature	600 to 700°C	Adherence versus activity
BET surface area	60 to 240 m^2/g	Catalyst activity
Ceramic loading	4 to 40% by weight	Catalyst activity, pressure drop
Active Metal		
Active metal	Iridium, Ruthenium	Catalyst activity, cost
Active metal loading	4 to 17% by weight 0.05 to 0.3 g Ir/cm^3 15 to 50% in activated coating	Catalyst activity
Hydrogen chemisorption	100 to 240 μ Moles/g	Catalyst activity

the sample. Also, thick layers of ceramic are more susceptible to cracking and flaking. The BET surface area was used as a guideline to evaluate different ceramic coatings and methods of ceramic coating application.

The range of active metals studied was limited to iridium and ruthenium. The amount of active metal in the catalyst, another important parameter, can be expressed in three different ways: percent by weight in the overall sample, volume-specific loading of the overall sample, and percent by weight active metal in the activated ceramic coating. This sequence is also the chronological order in which the three parameters were used to zero in on an optimum active metal loading.

Initially, percent by weight active metal was used, but then it became difficult to compare Hastelloy X with tungsten. Therefore, the volume specific loading was used instead, which is independent of

the type of foam metal in the matrix. Later, the percent active metal in the activated ceramic coating was optimized to avoid overloading the active surface area and plugging micropores, but still making maximum use of the available surface area on the ceramic. Typical active metal contents are now between 30 and 40% in the ceramic, which is also representative for commercially available hydrazine decomposition catalysts.

The hydrogen chemisorption was used as a guideline to evaluate methods of active metal deposition and to assess the effect of test firings on catalyst durability. Ignition was measured in a specially developed ignition delay tester to evaluate catalyst activity of experimental samples prior to preparing full-scale samples for reactor firings. This method was more economical and time saving.

During this program, too many parameters were varied; and reproducibility in reactor performance for identical sampies was not yet demonstrated, even though duplicate and triplicate samples were available in some cases. After some manual skill was developed and all parameters were carefully controlled, catalyst samples with reproducible properties could be prepared. The major variable is the amount of ceramic material deposited. With four W 210-7 samples in two batches, ceramic loading varied from 17.4 to 19.1%. Active metal content in the activated coating varied from 36.4 to 37.1% for a series of three samples in the same batch.

4.0 REACTOR TEST FIRINGS

4.1 GENERAL

Test firings of the more promising monolithic catalysts were carried out in a 2.2-N (0.5-lbf) thrust level reactor. This reactor, originally developed for Shell 405 catalyst, is shown in Figure 4-1. A summary of the nominal operating conditions for the reactor is given in Table 4-1.

Table 4-1
2.2N TCA OPERATING CHARACTERISTICS

Performance	
Vacuum thrust, N (lbf)	2.2 (0.5)
Propellant feed pressure, kN/m^2 (psia)	2482 (360)
Chamber pressure, kN/m^2 (psia)	1379 (200)
Vacuum specific impulse, N-sec/kg (lbf-sec/lbm)	2177 (222)
Nozzle expansion ratio	100:1
Bed loading, kg/m^2-sec (lbm/in^2-sec)	0.0000293 (0.01)
Characteristic velocity m/sec (ft/sec)	1274 (4180)
Catalyst bed	
Bed diameter, cm (in.)	1.265 (0.498)
Bed length, cm (in.)	2.0 (0.785)
Materials	
Thrust chamber	347 Stainless steel
Injector	347 Stainless steel
Capillary feed tube	Inconel 600
Thermal standoffs	AM 355

As shown in Figure 4-1, the injector assembly is flanged to the chamber body to permit easy inspection and replacement of the catalyst bed. Sealing of the injector to the chamber is accomplished by an asbestos-filled copper jacketed gasket. The injector consists of two flanges separated and held together by three tubular thermal standoffs and a capillary feed tube. The propellant valve screws into the modified AN fitting at the upper injector flange. An orifice is also contained in the injector inlet flange. The capillary feed tube injects the propellant into the catalyst bed. The top of the catalyst bed contains two screens, a 60- by 60-mesh screen followed by a 100- by 100-mesh screen, which is used to break up the propellant stream.

EXPLODED VIEW OF 2.2 N (0.5 lbf) REACTOR
WITH MONOLITHIC CATALYST AND INJECTOR HEAD

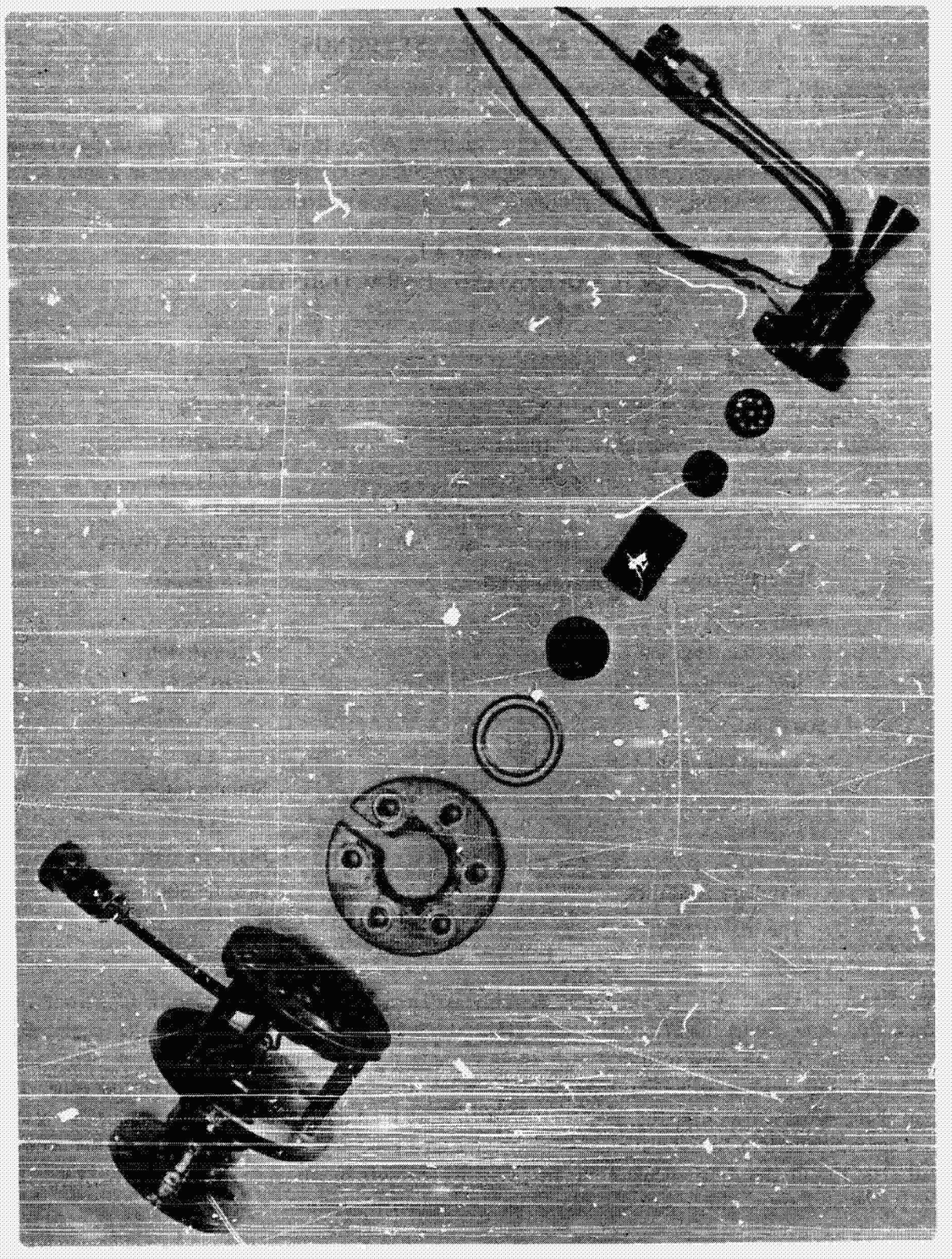

56000-38

Figure 4-1

The catalyst chamber is 1.27 centimeters (0.50 inch) in diameter and 2 centimeters (0.785 inch) long. Since parametric testing was not to be conducted during the testing, the bed length was fixed at that which gave satisfactory operation with Shell 405 catalyst. The walls of the thrust chamber were coated with a 0.05-centimeter (0.020-inch) thickness of Rockide Z (zirconium oxide) to minimize heat losses. The catalyst bed is retained on the downstream end by a perforated bed plate on the upstream surface to which is attached a 50- by 50-wire-mesh screen.

4.2 SUMMARY OF TEST FIRINGS

The 2.2-N (0.5-lbf) reactor test firings were used to conduct limited screening of catalysts for comparison of activity levels with laboratory scale tests, to conduct evaluation of the effect of variable metal loading and ceramic loading on catalyst performance and to evaluate the effect of foam metal pore size and metal type on catalyst performance. The tests conducted during the program are listed in Table 4-2 including characteristics of catalyst tested and test results. The ensuing sections summarize the results of these reactor tests in areas of (1) ceramic coating and metal loading, (2) foam metal material, and (3) foam metal pore size.

4.3 CERAMIC COATING AND METAL LOADING CONTENT

Initial tests conducted on monolithic catalysts used an aluminum oxide which was coated on by Astromet. This coating thickness was very thinly dispersed on the metal foam. Initial test evaluation (tests 001 through 008 in Table 4-2) of this catalyst indicated an adherence problem with the Astromet aluminum oxide. This problem, coupled by the lack of future availability of the aluminum oxide used by Astromet, resulted in RRC's undertaking an in-house development of coating the metal foam with high surface area ceramic.

A series of tests was conducted to evaluate the effect of variable ceramic coating thickness and ceramic active metal loading upon the performance characteristics of the catalyst. Results of these tests indicate that the optimum ceramic loading upon the 7% density foam metal is approximately 0.3 g/cm^3 of bed volume. The active metal loading which appears optimum with this ceramic loading is approximately 33 to 35% by weight active metal on the activated ceramic (i.e., 33 to 35% of total ceramic and active metal weight).

For comparison, 25- to 30-mesh ABSG Shell 405 catalyst with a bulk density of 1.45 g/cm^3 contains 33 ± 1% by weight iridium. The bulk active metal density is 0.47 g/cm^3; the bulk ceramic density is 0.98 g/cm^3.

Tests 028 through 037 represent test data on the baseline catalyst ceramic density and metal loading. Figure 4-2 plots the chamber pressure transient for selected tests throughout the test series. As noted, a progressive increase in the pressure rise time was noted throughout the test series. As will later be discussed, this was thought to be the result of marginality in the 20-mil pore size foam material.

Figure 4-3 plots the ignition characteristics of the test series as a function of start number. As shown by the data in the figure the ignition delay time appears to stabilize at around 80 milliseconds.

PRECEDING PAGE BLANK NOT FILMED

FOLDOUT FRAME 1

Table 4-2 —— 2.2-N (0.5-lbf) ENGINE TEST S

Test No	Foam Characteristics				Ceramic Loading (g/cm³)	Active Metal in Coating (%)	Prefire Weight (g)	Post-Fire Weight (g)	Response Time		Tailoff Time		Test Time (Sec)	Feed Pressure (kN m⁻²)
	Material	Type	Lot & Sample No.	Density (%)					Start P_c Rise (ms)	90% P_c (ms)	Start Decay (ms)	10% P_c (ms)		
001	Hastelloy X	230-15	32-76O	10.6		55.9	3.916		150				500	
002	Hastelloy X	230-15	32-76O			55.9		4.045	80				500	
003	Hastelloy X	230-15	32-76N	14.8	0.0 1		3.839		40				500	
004	Hastelloy X	230-15	32-76N		0.071			3.843	200				500	
005	Molybdenum	220-7	14	7.1	0.139		2.442		35				500	
006	Molybdenum	220-7	14		0.139			2.344	80				500	
007	Tungsten	230-15	32-75Q	10.7	0.067	46.6	4.876		360				5	
008	Tungsten	230-15	32-75Q		0.067	46.6		4.710					0	
009	Tungsten	220-7	7	7.0	0.731	17.01	1.7044	1.593	60				300	
010	Tungsten	230-15	32-75B	15.7	0.13	26.3	3.627	3.544	30				15	
011	Tungsten	230-15	W32-75R	10.6	0.318	22.1	5.660		40				500	
012	↓	↓	↓		↓	↓	↓		80				100	
013									100				100	
014									200				35	
015								5.543	200				35	
016	Hastelloy X	220-7	34-121.7A	5.9	0.375	31.95	2.588	2.605	47	44.850			200	2.730
017	Hastelloy X	220-7	34-121.5A	6.2	0.36	31.30	2.529		59	3.750	44	143	150	3.103
018	Hastelloy X	220-7	34-121.5A		0.36	31.30		2.453	72	23.000	50	157	100	3.123
021	Hastelloy X	220-7	34-121.10B	5.8	0.19	28.99	1.903	1.927	82	719	81	375	100	2.958
022	Hastelloy X	220-7	34-121.13B	5.3	0.23	19.23	1.745	1.749	60	952	30	233	100	3.041
023	Hastelloy X	220-7	34-121.12B	6.7	0.25	29.28	2.297		82	833	40	150	100	3.096
024	↓	↓	↓		↓	↓	↓		63	758	46	264	100	3.068
025									67	705	56	202	500	3.089
026									48	818	59	219	500	3.082
027								2.098	55	841	83	215	500	3.116
028	Hastelloy X	220-7	34-121.11B	5.2	0.22	37.84	1.916	N/M	30	347	69	153	100	2.654
029	↓	↓	↓		↓	↓	↓	↓	47	846	122	227	100	2.489
030									61	770	78	190	100	2.689
031									79	840	77	207	100	2.682
032									67	679	97	244	100	2.668
033									67	641	105	206	100	2.689
034									77	826	95	188	100	2.696
035									94	783	65	196	100	2.606
036									53	951	27	174	100	2.620
037									88	1.070	12	87	100	2.675
038	Tungsten	220-7	32-144.1	6.8	0.27	28.75	4.274		50	1.172	52	603	100	2.654
039	↓	↓	↓		↓	↓	↓		207	817	52	1.360	500	2.448
040								4.173	65	930	50	–	100	2.303
042	Hastelloy X	210-7	34-210.2B	8.9	0.41	36.13	1.687		24	1.110	8	1.133	500	2.461
043	↓	220-7	34-171.8B	6.8	0.23	37.10	1.239		38	715	2	560	500	2.448
044		↓	↓		↓	↓	↓		63	642	5	737	515	2.468
045									50	775	3	640	500	2.455
046									45	750	6	698	500	2.482
047									45	830	10	576	500	2.482
048								1.667	46	900	12	1.274	500	2.448
049								1.231	62	960	16	1.070	500	2.661
050	Tungsten	220-3.4	34-91B.16	3.4	0.26	29.53	2.612		55	2.740	28	1.748	500	2.482
051	Tungsten	220-3.4	34-91B.16		0.26	29.53		2.350	48	1.810	80	1.614	55	2.482
052	Tungsten	230-15	30-190B.27	11.0	0.21	34.04	6.402	6.332	62	1.840	37	–	150	2.544
053	Hastelloy X	220-7	32-171.4A	7.9	0.30	34.03	2.863		243	479	30	245	500	2.510
054	↓	↓	↓		↓	↓	↓		122	810	32	795	100	2.510
055									170	770	27	870	100	2.517
056								2.847	428	678	29	710	100	2.510
057	Hastelloy X	210-7	34-210.1A	8.5	0.446	33.10	1.580	1.562	25	963	6	693	100	2.489
058	Hastelloy X	210-7	34-210.3D	9.5	0.535	35.85	1.652	1.627	30	1.120	–	–	100	2.489
059	Tungsten	220-7	32-144.3	7.0	0.261	35.79	4.294		31	1.002	20	830	100	2.482
060	Tungsten	220-7	32-144.3	7.0	0.261	35.79		4.211	51	990	22	742	100	2.503
061	Tungsten	220-7	32-197A.1	6.2	0.292	34.02	4.191		37	2.000	40	1.780	500	2.461
062	↓	↓	↓		↓	↓	↓		18	1.420	34	–	500	2.461
063									38	1.728	32	1.270	500	2.517
064									18	1.518	50	–	500	2.475
065									20	1.575	15	–	500	2.468
066									30	1.465	44	790	500	2.448
067									32	1.350	45	1.130	500	2.448
068									9	1.413	38	920	500	2.448
069									60	1.325	–	–	500	2.461
070									49	1.185	41	775	500	2.448
071									50	1.202	–	–	100	2.461
072									62	1.186	43	965	500	2.461
073									45	1.608	39	1.370	500	2.448
074									49	1.500	–	–	500	2.468
075									50	1.790	52	152	500	2.461
076									82	1.954	55	910	500	2.448
077	↓	↓	↓		↓	↓	↓	4.051	79	1.152	–	–	100	2.482

FOLDOUT FRAME 2

Table 4-2 — 2.2-N (0.5-lbf) ENGINE TEST SUMMARY

Response Time		Tailoff Time		Test Time (Sec)	Feed Pressure (kN/m²)	Chamber Pressure (kN/m²)	Pressure Oscillations (kN m²)		c* (m sec)	Bed Pressure Drop (kN m²)	Remarks
	90% P_c (ms)	Start Decay (ms)	10% P_c (ms)				Maximum	Nominal			
				500						N M	Ashcroft ceramic
				500						N M	
				500						N M	Ashcroft ceramic
				500						N M	
				500						N M	Ashcroft ceramic
				500						N M	
				5						N M	Ashcroft ceramic
				0						N M	
				300						N M	RK ceramic for remainder tests
				15						N M	
				500						N M	
				100							
				100							
				35							
				35							
	44.850			200	2.730	1.076	137.9	72 1	1.254	N/M	
	3.750	44	143	150	3.103	1.172	81.0	56.9	1.224	N/M	
	23.000	50	157	100	3.123	1.165	44.8	19.0	1.213	N/M	
	719	81	275	100	2.958	1.131	65.5	17.2	1.185	N/M	
	952	30	233	100	3.041	1.096	155.1	72.4	1.148	N/M	
	833	40	190	100	3.096	1.172	63.8	17 2	1.227	N/M	
	758	46	164	100	3.068	1.179	62.1	27 6	1.233		
	705	56	202	500	3.089	1.172	68.9	34.5	1.230		
	818	59	219	500	3.082	1.172	131.0	34.5	1.251		
	841	83	215	500	3.116	1.186	103.4	27.6	1.269		
	747	69	153	100	2.654	1.517	41.4	17.9	1.186	N/M	
	846	122	227	100	2.489	1.020	51.0	21.4	1.181		
	770	78	190	100	2.689	1.048	36.5	17.2	1.182		
	840	77	207	100	2.682	1.089	36.5	17.2	1.180		
	679	97	244	100	2.668	1.027	22.8	13.1	1.159		
	641	105	206	100	2.689	1.048	34.5	15.9	1.183		
	826	95	188	100	2.696	1.076	30.3	16.5	1.226		
	783	65	196	100	2.606	1.096	43.4	5.5	1.228		
	951	27	174	100	2.620	1.069	20.7	8.6	1.185		
	1.070	12	87	100	2.606	883	12.1	6.9	1.202		
	1.172	52	603	100	2.654	1.538	206.8	86.2	1.224	55.2	
	817	52	1.360	500	2.448	1.551	406.8	296.5	1.238	N/M	
	930	50	–	100	2.303	1.517	441.3	399.9	1.225	N/M	
	1.110	8	1.133	500	2.461	1.441	75.8	34.5	1.198	68.9	
	715	2	560	500	2.448	1.434	20.7	13.8	1.207	89.6	
	642	5	737	515	2.468	1.448	41.4	20.7	1.203	89.6	
	775	3	640	500	2.455	1.427	34.5	20.7	1.237	89.6	
	750	6	698	500	2.482	1.448	34.5	20.7	1.156	89.6	
	830	10	570	500	2.482	1.455	41.4	20.7	1.194	82.7	
	900	12	1.274	500	2.448	1.441	103.4	34.5	1.193	96.5	
	960	16	1.070	500	2.661	1.455	75.8	34.5	1.185	89.6	
	2.740	28	1.748	500	2.482	1.434	296.5	48.3	1.159	41.4	
	1.810	80	1.614	55	2.482	1.344	448.2	310.3	1.052	48.3	
	1.850	37	–	150	2.544	1.489	655.0	489.5	1.157	–	
	479	30	245	500	2.510	1.179	82 7	20.7	916	441.3	Ruthenium active metal
	810	32	795	100	2.510	1.124	62.1	20.7	915	406.8	
	770	27	870	100	2.517	1.124	34.5	20.7	908	399.9	
	678	29	710	100	2.510	1.117	68.9	13.8	–	13.8	
	963	6	693	100	2.489	1.469	31.0	15.9	1.198	51.7	
	1.120	–	–	100	2.489	1.475	35.9	24.1	1.226	51.7	
	1.002	20	830	100	2.482	1.517	103.4	34.5	1.225	10.3	
	930	22	742	100	2.503	1.531	129.7	34 5	1.246	20.7	
	2.090	40	1.780	500	2.461	1.269	144.8	17.2	–	27.6	
	1.420	34	–	500	2.461	1.344	117.2	20.7	1.257	20.7	
	1.718	33	1.270	500	2.517	1.276	68.9	17.9	1.193	13.8	
	1.518	50	–	500	2.475	1.289	172.4	17.2	1.255	27.6	
	1.575	43	–	500	2.468	1.289	124.1	20.7	1.206	27.6	
	1.465	44	790	500	2.448	1.269	103.4	17.2	1.244	20.7	
	1.350	45	1.130	500	2.448	1.255	110.3	17.2	1.179	27.6	
	1.413	38	920	500	2.448	1.276	68.9	24.2	1.250	41.4	
	1.326	–	–	500	2.461	1.276	82 7	34.5	1.250	34.5	
	1.185	41	775	5[illegible]	2.448	1.276	82 7	34.5	1.233	27.6	
	1.202	–	–		2.461	1.282	82.7	41.4	1.241	27.6	
	1.186	43	965	500	2.461	1.089	82 7	34.5	1.260	13.8	
	1.608	39	1.370	500	2.448	1.089	75.8	34.5	1.250	20.7	
	1.500	–	–	500	2.468	1.103	75.8	34.5	1.255	20.7	
	1.796	52	152	500	2.461	1.103	82 7	17.2	1.259	27.6	
	1.954	55	110	500	2.448	1.131	103.4	17.9	1.256	20.7	
	1.152	–	–	100	2.482	1.89	68.9	20.7	1.215	20.7	

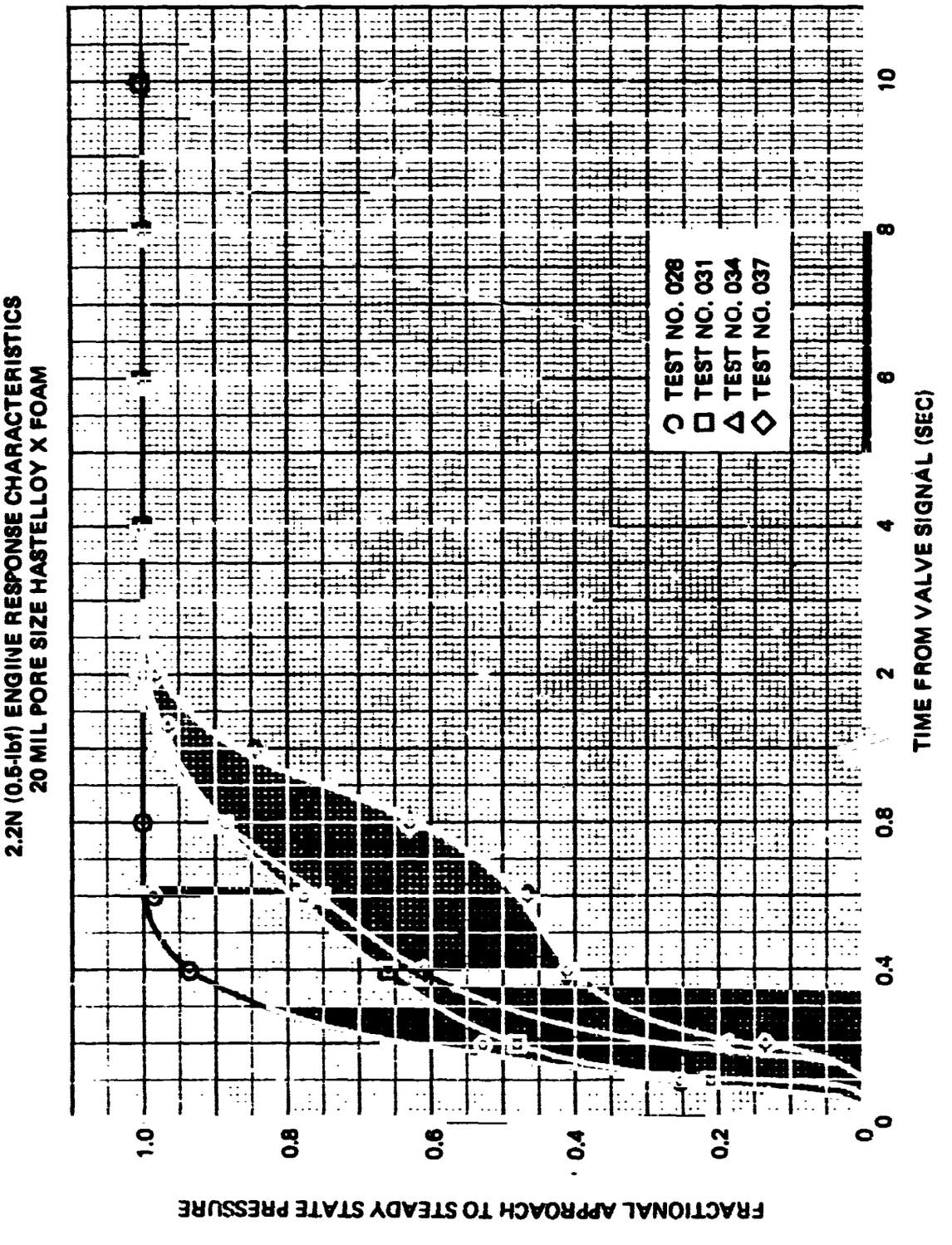

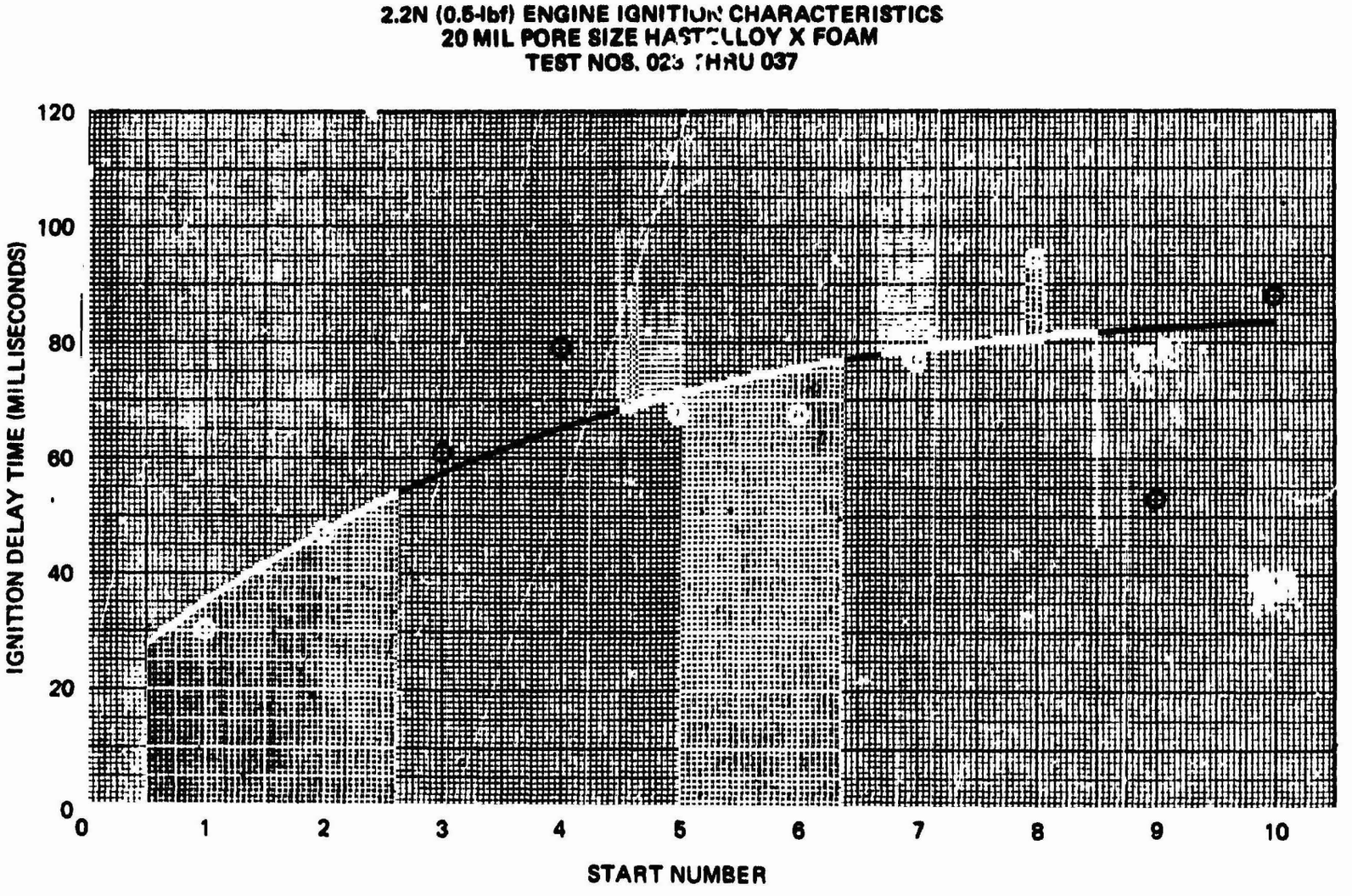
2.2N (0.5-lbf) ENGINE IGNITION CHARACTERISTICS
20 MIL PORE SIZE HASTELLOY X FOAM
TEST NOS. 023 THRU 037
IGNITION DELAY TIME (MILLISECONDS)
120
100
80
60
40
20
0
0
1
2
3
4
5
6
7
8
9
10
START NUMBER

Figure 4-3

As is noted by the data summary in Table 4-2, chamber pressure oscillations were low in all tests. Each test was 100 seconds in duration, with the total test time limited to preclude severe nitriding in the cases of the Hastelloy X foam.

4.4 FOAM METAL

The majority of the testing conducted on the first phase of work was with foam metal made from Hastelloy X material. Early in the program test data indicated rather severe nitriding and subsequent breakup of the Hastelloy X foam material after 3,000 to 4,000 seconds of operation. Hastelloy X was then regarded as an interim material used for evaluation of variable ceramic and active metal loading. Development work was initiated to develop a foam metal which was inert to the decomposition gas environment. Evaluation of materials had narrowed this selection down to molybdenum or tungsten. Molybdenum foam metals exhibited no advantage so that effort was concentrated upon development of acceptable tungsten foam metal in a nominal 7% theoretical density. Astromet Associates, Incorporated, was responsible for the fabrication of the foam metals.

Toward the end of the program, acceptable foam metals made of tungsten (acceptable in terms of strength and density) were fabricated by Astromet. Initial evaluation of the improved tungsten foam resulted in very unsatisfactory reactor operation. Near-flooding and high-pressure oscillations were encountered (see tests 050 through 060 in Table 4-2). Examination of the catalysts made on the tungsten foam revealed that the aluminum oxide was not adhering to the foam metal surface. Comparison of the tungsten foam with the Hastelloy X foam, which had given satisfactory aluminum oxide adherence, indicated that the tungsten foam surface was very smooth. The Hastelloy X surface had a rough texture which was felt to provide adherence of the aluminum oxide.

Means were sought to roughen the tungsten surface. Two techniques were arrived at for evaluation. One consisted of oxidizing the tungsten and the second was to sinter tungsten powder to the foam surface. Oxidation treatment of the foam did result in roughening of the surface but the strength was reduced markedly. Sintering of tungsten powder on the surface of the foam appeared to provide a roughened surface characteristic which was equal to that which existed on the Hastelloy X. Catalysts were prepared on this foam material for evaluation in the 0.5-lbf reactor.

A total of 16 tests totaling 7,700 seconds burn time were accumulated on the catalyst made on the tungsten foam which had been surface roughened by sintering on tungsten metal powder. These tests were summarized in Table 4-2 as tests 062 through 077. Very satisfactory operation was achieved in all tests. The drop-off in chamber pressure noted in tests 072 through 077 was found to be caused by plugging of an upstream orifice in the test system and not by any change in the catalyst bed. Examination of the catalyst after test 077 indicated no structural change in the foam metal. All ligaments were intact. A weight loss of 5.4% occurred as a result of the 16 tests, totaling 7,700 seconds burn time. Some of this weight loss may be attributed to handling losses while the catalyst was being inserted and removed from the reactor.

Figure 4-4 plots the chamber pressure start transient versus burn time for selected starts at the beginning, middle, and end of the test series. As shown in the figure the time to 90% does not vary significantly throughout the test series, but the slope of the pressure-time curve up to 90% varies with accumulated burn time. It is expected that the shape of this curve will improve markedly by a change to 10-mil pore-size foam material.

Figure 4-5 plots chamber pressure roughness versus accumulated test time for the test series. As noted, no increase in pressure oscillations are noted throughout the test series. In fact, the maximum levels actually decrease slightly and become more consistent as burn time is accumulated.

The ignition delay characteristics obtained during the test series are plotted in Figure 4-6 as a function of start number. Although there is a trend of increasing ignition delay with number of starts, the delay time is comparable to Shell 405 catalyst.

4.5 METAL FOAM PORE SIZE

The average pore size of monolithic foam structure was a very important variable in terms of engine firing test results obtained. Completely unacceptable firings were obtained with 30-mil pore-size foam. Near flooding or lack of ignition was encountered in all firings with 30-mil pore-size material. The major portion of the program used 20-mil pore-size foam. With proper ceramic coating, metal loading, and ceramic adhesion, acceptable steady-state operation with acceptable pressure oscillations were obtained. However, during all testing with 20-mil pore-size foam, trends were established to indicate that this pore size, at least for the total bed, is marginal. These are:

a. An increase in the time from ignition to 10% of steady-state chamber pressure.

b. A substantial time from valve close to start of chamber pressure decay and a long pressure decay transient.

Both of the above two items are indicative of liquid penetration down along the top portion of the monolithic catalyst bed.

The unacceptable operation with the 30-mil pore-size material and the somewhat marginal operation with 20-mil pore-size foam is believed due to channeling of the propellant through the bed with the larger pore-size material. To test the effect of smaller pore size on reactor operation, a layered bed of one-half 10-mil pore size on top followed by one-half 20-mil pore size was tested. These tests are given by tests 042 through 049. As noted in the data summary of Table 4-2, response times and decay times are very consistent throughout the test series. Additionally, the time from valve close to start of pressure decay is reduced from approximately 50 milliseconds to a value of 5 to 10 milliseconds, which indicates much less liquid penetration into the catalyst bed. Chamber pressure oscillations are also markedly reduced by use of the 10-mil pore-size foam for the top portion of the bed.

Figure 4-7 plots the chamber transient for selected tests in the series of eight conducted with the 10/20-mil pore-size bed. As noted, extremely repeatable response characteristics were obtained over the eight tests covering some total of 4,000 seconds burn time. No pressure overshoot on starting

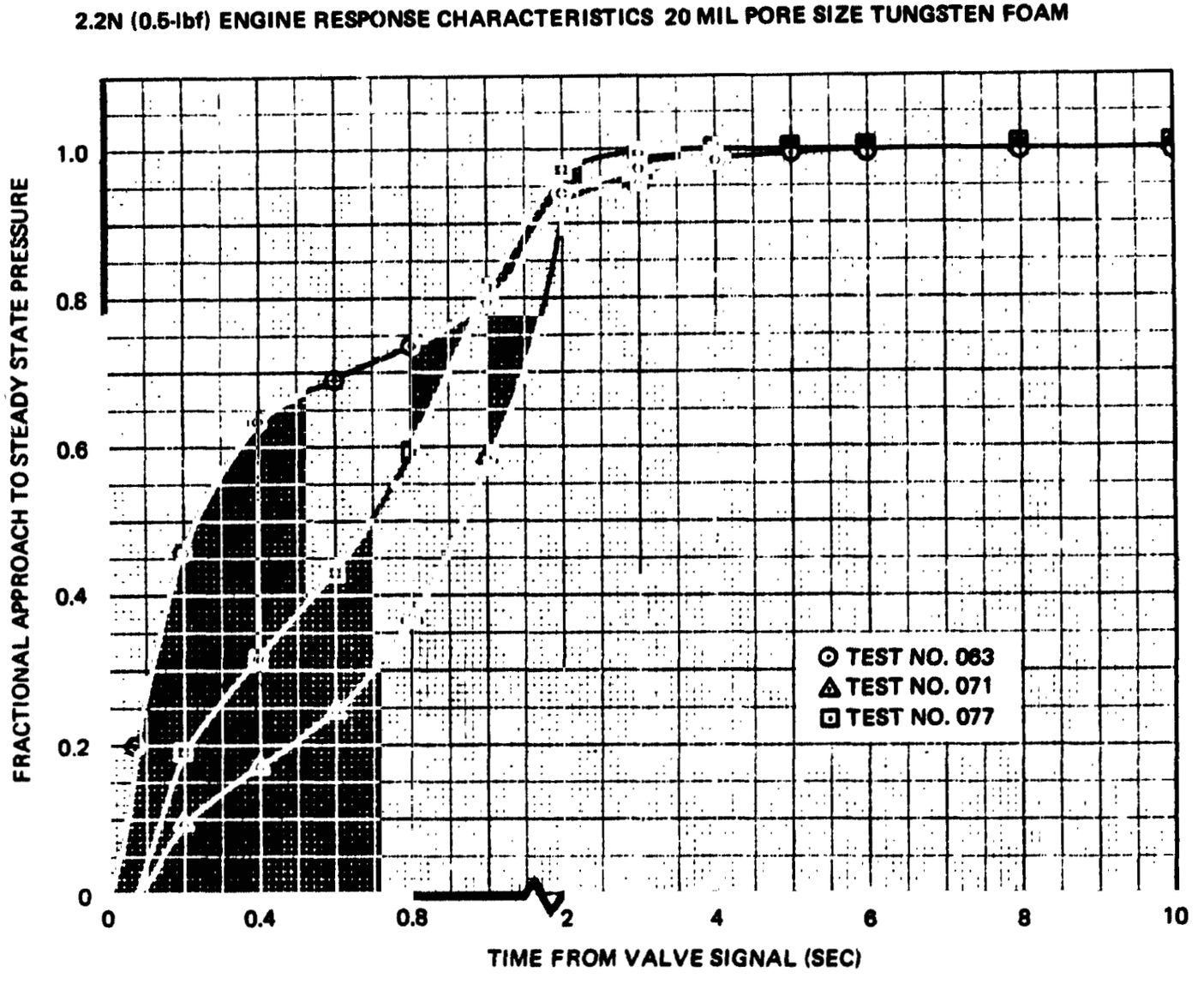
2.2N (0.5-lbf) ENGINE RESPONSE CHARACTERISTICS 20 MIL PORE SIZE TUNGSTEN FOAM
FRACTIONAL APPROACH TO STEADY STATE PRESSURE
1.0
0.8
0.6
0.4
0.2
0
0
0.4
0.8
2
4
6
8
10
TIME FROM VALVE SIGNAL (SEC)
TEST NO. 063
TEST NO. 071
TEST NO. 077

Figure 4-4

2.2N (0.5-lbf) ENGINE PRESSURE OSCILLATIONS, TEST NOS. 062 THRU 077
20 MIL PORE SIZE TUNGSTEN FOAM
PEAK-TO-PEAK PRESSURE OSCILLATIONS (psia)
±25
±20
±15
±10
±5
0
0
2000
4000
6000
8000
ACCUMULATED TEST TIME (SECONDS)

Figure 4-5

2.2N (0.5-lbf) ENGINE IGNITION CHARACTERISTICS
20 MIL PORE SIZE TUNGSTEN FOAM
TEST NOS. 062 THRU 077

Figure 4-6

2.2N (0.5-lbf) ENGINE RESPONSE CHARACTERISTICS
10 MIL PORE SIZE UPPER BED/20 MIL PORE SIZE LOWER BED
FRACTIONAL APPROACH TO STEADY STATE PRESSURE
1.0
0.8
0.6
0.4
0.2
0
0
0.4
0.8
2
4
6
8
10
TIME FROM VALVE SIGNAL (SECONDS)
TEST NO. 043
TEST NO. 047
TEST NO. 049

Figure 4-7

was encountered. Figure 4-8 plots pressure oscillations as a function of accumulated burn time for the eight tests (each of 500 seconds' duration). As noted, pressure oscillations were very low (approximately ± 5 psid or ± 2%) until about 3,000 seconds burn time, when they increased markedly. The increase was caused by breakup of the Hastelloy X metal foam due to nitriding. This trend is also seen in Figure 4-9 wherein response time to 90% and tailoff time to 10% is plotted as a function of start number. For the last two starts, response and tailoff times both increased, which indicated a void in the bed. The relatively long tailoff time is due to the high holdup volume between the valve and catalyst bed.

Tests 057 and 058 were conducted with a total bed of 10-mil pore-size foam. Operation was similar to that of the layered bed tests above except for a slightly higher bed pressure drop which is expected with the all 10-mil pore-size bed. The mean pore size appears to be analogous, and to give similar performance, to using fine mesh catalyst at the top of a granular catalyst bed.

2.2N (0.5-lbf) ENGINE PRESSURE OSCILLATIONS
TEST NOS. 042 THRU 049
PEAK-TO-PEAK PRESSURE OSCILLATIONS (psia)
±20
±16
±12
±8
±4
±0
0
1000
2000
3000
4000
ACCUMULATED BURN TIME (SECONDS)

Figure 4-8

2.2N (0.5-lbf) ENGINE RESPONSE CHARACTERISTICS
10 MIL PORE SIZE UPPER BED 20 MIL PORE SIZE LOWER BED
TEST NOS. 042 THRU 049

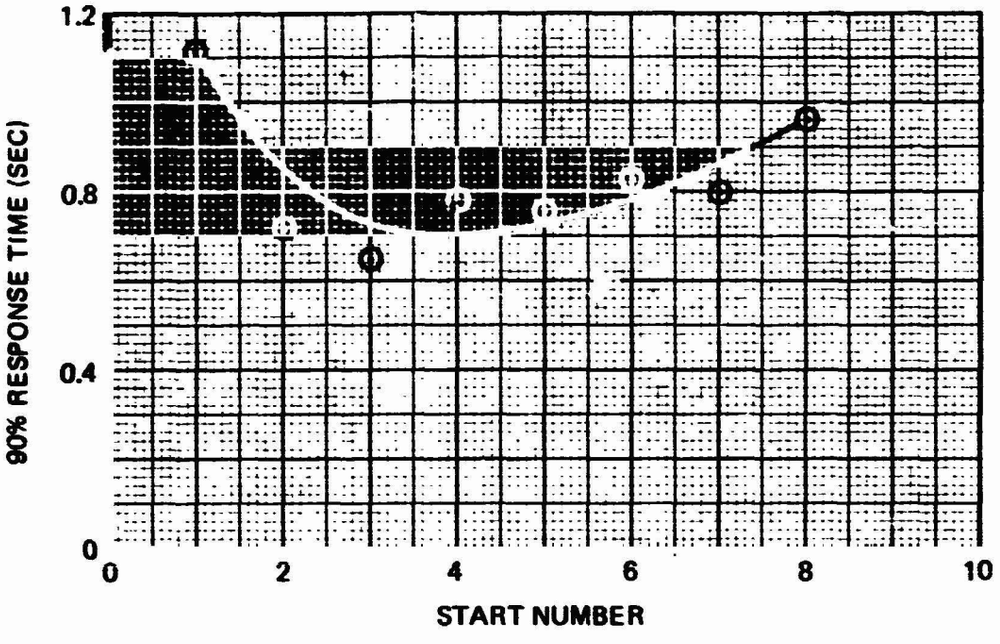

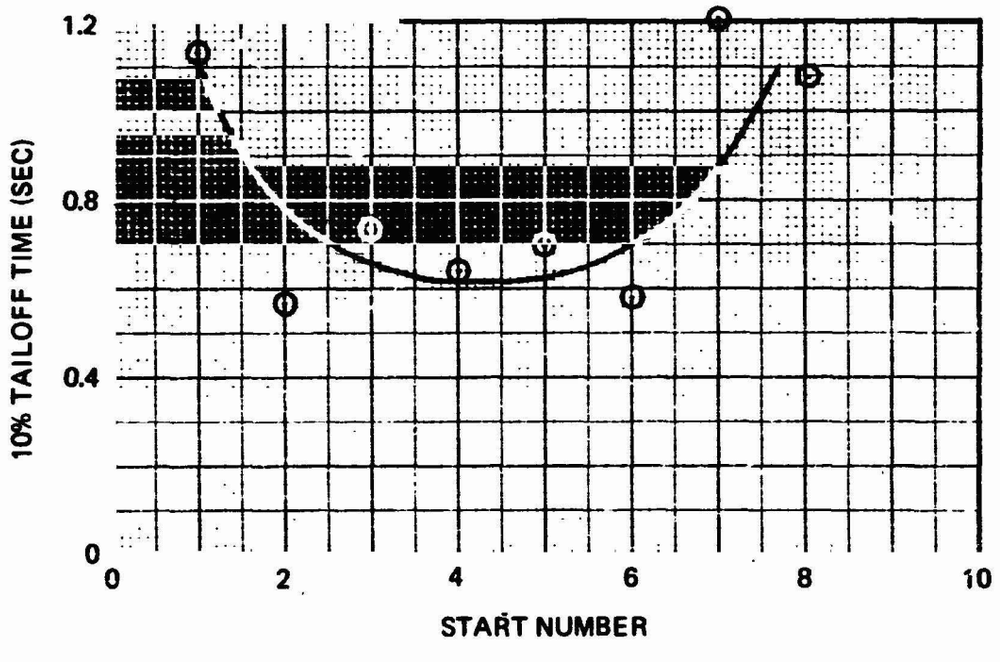

5.0 CONCLUSIONS AND RECOMMENDATIONS

The basic feasibility of developing a monolithic catalyst bed which has a catalytic activity comparable to Shell 405 has been demonstrated under the program. The development of a catalyst comprising iridium-promoted, silica-stabilized alumina coatings on a metal foam substrate has given catalytic properties which result in cold bed ignition delay times comparable to Shell 405. One of the main advantages of this catalyst which appears in the cold start pressure transient is a lack of pressure overshoot.

It may well be that a finally optimized catalyst will not be as susceptible to cold start degradation as is Shell 405.

Two problem areas were uncovered during the program with the metal foam substrates. The Hastelloy materials performed well initially but became severely nitrided after approximately 3,000 seconds of operation in the reactor, with a resultant limitation of their lifetimes. In testing conducted towards the end of the program, tungsten was found not subject to nitriding but susceptible to coating adhesion problems. A possible solution to this problem was indicated by roughening of the tungsten surface.

It is believed that the results of the initial phase of research are encouraging and that additional work should be conducted and aimed at finalizing the development of this catalyst. The major objective of the additional work should be to:

a. Obtain a nitridation-resistant substrate through either a second metal deposition to provide chemical inertness on additional evaluation of refractory metals.

b. Finalize suitable substrate surface preparation techniques to ensure adhesion of the promoted alumina coating.

c. Finalize the catalyst formulation with detailed documentation of fabrication techniques and processes.

Upon completion of items a. through c. above, it is recommended that selected scaling studies of variable bed loading, bed length, and chamber pressure be conducted to more fully characterize the catalyst. These studies should then be followed by life-test evaluation for comparison with the present capabilities of Shell 405 catalyst.

REFERENCES

1. 1971 Materials Selector Issue, Materials Engineering, Reinhold Publishing Corporation.

2. Carlson, R. A., Blumenthal, and Grassi, R. J.: *Space Environment Operation of Experimental Hydrazine Reactors*, Interim Tech Summary Report, TRW Systems, Contract NAS 7-520 (January 30, 1968).

3. Good, C. D., Poole, D. R., and Schmidt, E. W.: *Reaction Engine Module Monopropellant, Shell 405 Catalyst Experience*, Rocket Research Corporation 67-ES-54 (December 1967).

APPENDIX
NOMENCLATURE

Pore Size

There are several systems in use to describe geometry and density of open-cell foams. Some manufacturers give the pore size in pores per inch (ppi). Other manufacturers give the pore diameter in thousands of an inch (mils) or micrometers (1 mil - 25.4 μm). It is necessary to differentiate between pore diameter and window diameter. The ratio between pore and window diameter may vary between 2 and 20.

Density

Percent density is the percent of density of a solid piece of metal of equal outside dimensions. Example: a cylinder of solid tungsten, 0.5-inch diameter by 0.785-inch length weighs 48.87 grams. A foam sample of the same outside dimensions weighing 4.89 grams has a density of 10%. The percent void volume is 100% minus percent density.

Astromet Nomenclature

Astromet Associates uses a code which gives both pore diameter and percent density, e.g.:sINSERT,

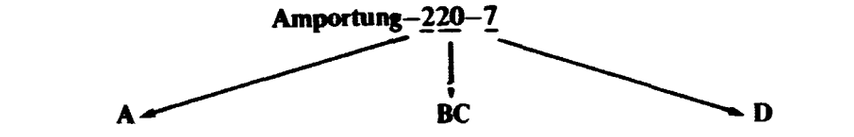

A = Foam structure BC = Pore diameter in mils D = % density

1 Blocky spherical
2 Light Tetrahedra
3 Heavy tetrahedra

Macroporosity

This is porosity visible to the naked eye due to the foam structure. The surface due to macroporosity is called geometrical surface area.

Microporosity

This denotes micropores in the ceramic coating. Surface area in these pores is called active surface area or BET surface area.